(12) INTERNATIONAL APPLICATION PUBLISHED UNDER THE PATENT COOPERATION TREATY (PCT)

(19) World Intellectual Property Organization
International Bureau

(43) International Publication Date
11 May 2018 (11.05.2018)

WIPO | PCT

(10) International Publication Number
WO 2018/085622 A1

(51) International Patent Classification:
A61L 27/00 (2006.01) *C12N 5/071* (2010.01)
C12N 5/00 (2006.01)

(21) International Application Number:
PCT/US2017/059860

(22) International Filing Date:
03 November 2017 (03.11.2017)

(25) Filing Language: English

(26) Publication Language: English

(30) Priority Data:
62/417,371 04 November 2016 (04.11.2016) US
62/517,414 09 June 2017 (09.06.2017) US

(71) Applicant: **CHILDREN'S HOSPITAL MEDICAL CENTER** [US/US]; 3333 Burnett Avenue, Cincinnati, OH 45229 (US).

(72) Inventors: **TAKEBE, Takanori**; c/o 3333 Burnett Avenue, Cincinnati, OH 45229 (US). **OUCHI, Rie**; c/o 3333 Burnett Avenue, Cincinnati, OH 45229 (US). **KIMURA, Masaki**; c/o 3333 Burnett Avenue, Cincinnati, OH 45229 (US).

(74) Agent: **TEPE, Nicole, M.** et al.; Frost Brown Todd LLC, 3300 Great American Tower, 301 East Fourth Street, Cincinnati, OH 45202 (US).

(81) Designated States *(unless otherwise indicated, for every kind of national protection available)*: AE, AG, AL, AM, AO, AT, AU, AZ, BA, BB, BG, BH, BN, BR, BW, BY, BZ, CA, CH, CL, CN, CO, CR, CU, CZ, DE, DJ, DK, DM, DO, DZ, EC, EE, EG, ES, FI, GB, GD, GE, GH, GM, GT, HN, HR, HU, ID, IL, IN, IR, IS, JO, JP, KE, KG, KH, KN, KP, KR, KW, KZ, LA, LC, LK, LR, LS, LU, LY, MA, MD, ME, MG, MK, MN, MW, MX, MY, MZ, NA, NG, NI, NO, NZ, OM, PA, PE, PG, PH, PL, PT, QA, RO, RS, RU, RW, SA, SC, SD, SE, SG, SK, SL, SM, ST, SV, SY, TH, TJ, TM, TN, TR, TT, TZ, UA, UG, US, UZ, VC, VN, ZA, ZM, ZW.

(84) Designated States *(unless otherwise indicated, for every kind of regional protection available)*: ARIPO (BW, GH, GM, KE, LR, LS, MW, MZ, NA, RW, SD, SL, ST, SZ, TZ, UG, ZM, ZW), Eurasian (AM, AZ, BY, KG, KZ, RU, TJ, TM), European (AL, AT, BE, BG, CH, CY, CZ, DE, DK, EE, ES, FI, FR, GB, GR, HR, HU, IE, IS, IT, LT, LU, LV, MC, MK, MT, NL, NO, PL, PT, RO, RS, SE, SI, SK, SM, TR), OAPI (BF, BJ, CF, CG, CI, CM, GA, GN, GQ, GW, KM, ML, MR, NE, SN, TD, TG).

Declarations under Rule 4.17:
— *of inventorship (Rule 4.17(iv))*

Published:
— *with international search report (Art. 21(3))*

WO 2018/085622 A1

(54) Title: LIVER ORGANOID DISEASE MODELS AND METHODS OF MAKING AND USING SAME

(57) Abstract: Disclosed herein are methods of making and using lipotoxic organoid models. In certain aspects, the methods may comprise the steps of contacting a liver organoid with a free fatty acid (FFA) composition. In one aspect, the FFA composition may comprise oleic acid, linoleic acid, palmitic acid, or combinations thereof.

LIVER ORGANOID DISEASE MODELS AND METHODS OF MAKING AND USING SAME

Cross Reference to Related Applications

[0001] This application claims priority to and benefit of U.S. Provisional Patent Application 62/471,371, filed November 4, 2016, and 62/517,414, filed June 9, 2016, the contents of each are incorporated by reference in their entirety for all purposes.

Background

[0002] Irreversible epithelial organ remodeling is a major contributing factor to worldwide death and disease, costing healthcare systems billions of dollars every year (Hynds and Giangreco, 2013). Diseases of epithelial remodeling include lung and gastrointestinal cancers as well as chronic diseases such as liver cirrhosis, chronic obstructive pulmonary disease (COPD), and inflammatory bowel disease (Hynds and Giangreco, 2013). Sadly, most epithelial organ research performed primarily on animals fails to produce new therapies for these diseases and mortality rates remain unacceptably high. This is partly due to a lack of predictive human systems to test the efficacy of a vast growing number of compound libraries in pharmaceutical industries, imposing a fundamental challenge to develop a high-fidelity system for modeling inflammation and fibrosis in humans towards clinically relevant therapy development.

[0003] Non-alcoholic Fatty Liver Disease (NAFLD) is one of the major challenges to be overcome in developed countries due to the increased chance of developing lethal liver disorders, yet effective treatment is lacking. Similarly, iatrogenic parenteral nutrition associated liver disease (PNALD) is a disorder that

arises from parenteral nutrition and which currently has no effective treatment. Models having steatohepatitis and/or clinical histopathological features of liver disease such as lipid droplet accumulation and cystoskeleton filament disorganization, steatosis, and hepatocellular ballooning, and which can be used to address these and other liver disorders or disease states, are needed. Despite the promise of disease models using patients' stem cells, current approaches are limited in their applications to unicellular, monogenic and relatively simple pathologies, failing to capture more prevailing and complex disease pathology such as epithelial organ fibrosis.

[0004] The human liver is a vital organ that provides many essential metabolic functions for life such as lipid metabolism, ammonium and bile production, coagulation, as well as the detoxification of exogenous compounds. Using induced pluripotent stem cell (iPSC) technology, in vitro reconstitution of patients' liver reaction is attractive to the pharmaceutical industry, due to a number of promising applications including regenerative therapy, drug discovery, and drug toxicity studies. To this aim, currently, conventional *in vitro* approaches study two-dimensional (2-D) and 3-D differentiation platforms to generate liver cells. However, most of the reported methods predominantly differentiate cells into target epithelial cell type, completely lacking an essential supporting component such as pro-fibrotic and/or inflammatory cell types. Alternatively, Applicant and others have proposed co-culture based approaches by mixing epithelial and supportive lineages, however, these assays are heavily variable and often confounded by a number of artefactual changes such as the difficulty in selecting Epithelial Cell Medium (ECM) and medium in which they can be co-maintained. Thus, there is a need for the establishment of a new and robust assay

system in which the supportive lineages co-develop for disease modeling and further screening application.

Brief Summary

[0005] Disclosed herein are methods of making and using lipotoxic organoid models. In certain aspects, the methods may comprise the steps of contacting a liver organoid with a free fatty acid (FFA) composition. In one aspect, the FFA composition may comprise oleic acid, linoleic acid, palmitic acid, or combinations thereof.

Brief Description of the Drawings

[0006] Those of skill in the art will understand that the drawings, described below, are for illustrative purposes only. The drawings are not intended to limit the scope of the present teachings in any way.

[0007] The patent or application file contains at least one drawing executed in color. Copies of this patent or patent application publication with color drawing(s) will be provided by the Office upon request and payment of the necessary fee.

[0008] FIG 1. Co-differentiation of pre-fibrotic and inflammatory lineages in human iPSC-liver organoid A. Schematic representation of retinoic acid (RA)-based liver organoid differentiation method and bright-field image of day 20 liver organoids. Scale bar, 100 μm. B. Bright-field image of liver organoids in Matrigel at day 20 after the culture in the presence and absence of 4 days RA. C. Organoid numbers were measured manually at day 20 after the culture in the presence (black bar) and absence (gray bar) of 4 days RA. D. Diameter of organoid was recognized and measured by Image J at day 20 after the

culture in the presence (black bar) and absence (gray bar) of 4 days RA. E. Albumin production was measured from the culture supernatants collected in 24 hrs after the culture of day 22- 25 liver organoids in Matrigel with (black bar) or without (gray bar) 4 days RA. F. Organoids with internal luminal structure were counted manually at day 25 after culturing in the presence and absence of 4 days RA. Red and gray bars indicate the percent of organoids with (HLO) / without (spheroid) internal luminal structure, respectively. G. Bile transport activity was monitored by fluorescein diacetate (FD), which turns into fluorescein (green) after esterase hydrolysis in hepatocytes, in the culture media and tracks the flow of the fluorescence. Results represent mean ±s.d., n=3. Percentages of Epcam, CD166, and CD68 positive population were determined by flow cytometry. Results represent mean ±s.d., n=2-3. H. Single cell RNA sequencing!! FPKM (log2) values for hepatocyte, stellate cell, Kupffer cell, and endothelial-associated genes expressed by human iPSC, human iPSC derived definitive endoderm, foregut spheroid, HLO, human adult liver tissue and human fetal liver tissue. I. Percentages of Epcam, CD166, CD68, and F4/80 positive population were determined by flow cytometry. Results represent mean ±s.d., n=3. J. Immunofluorescent (IF) staining of day 25 HLO for albumin, CD68, Vimentin, GFAP and Epcam. White arrow indicates the localization of the cells positive for CD68, GFAP, and Vimentin. Results represent mean ±s.d., n=3. K. Phagocyte activity was analyzed by monitoring intracellular pH using pHrodo indicators that reflect phagocytosis (red). The fluorescent expression was captured under confocal microscopy. Results represent mean ±s.d., n=6.

[0009] FIG 2. Generation of steatohepatitis organoids (sHLO) by fatty acid treatment A. Schematic representing the method for

generating steatohepatitis HLO (sHLO) B. Live-cell imaging of lipid droplets (green), membrane (red), and nuclear (blue). The image was adopted from the overlay of 10-20 Z-stack images. Increase of lipid droplet accumulation and enlargement of lipid droplets and cells were observed in a dose depended manner. C. Representative total lipid volume normalized by each organoid size. Bar shows the mean of the total lipids volume. Lipid droplets were increased in a dose depended manner 0 (black), 200 μM OA (red), 400 μM OA (green), and 800 μM OA (blue). D. Quantification of triglycerides in HLO. HLOs were isolated from one Matrigel drop and divided into HCM media in the presence (blue bar) or absence (black bar) of oleic acid (800 μM) and cultured for 3 days. E. ELISA measurement of IL-6 with culture supernatants obtained from the wells that contain 20-30 HLO cultured in the presence or absence of oleic acid (800 μM) and cultured for 3 days. The final values were normalized by the number of organoids in each well. IL-6 was 2.2-fold released in 800 μM OA treatment (blue bar), when compared with non-treatment (black bar). F. Gene expression of pro-inflammatory cytokines TNF-alpha and IL-8. They were normalized by 18S. Both TNF-alpha and IL-8 gene expression were upregulated in 200 μM OA (red bar) and 800 μM OA (blue bar), compared with untreated (black bar). G. 10-20 HLO were cultured in HCM media including 0, 400, 800uM OA for 3 days. The cultured supernatants were collected from each well, and THP-1 migration was measured by using transmembrane with those supernatants. Cells that had migrated were counted and normalized by the exact number of organoids in each well. H. Trichrome staining of day 25 HLO and percentage of trichrome stained HLO on HLO (black bar), sHLO (red bar) and cHLO (blue bar) populations. Results represent mean ±s.d., n=8-20 organoids. I. IF staining of

day 25 HLO for Epcam and Vimentin and percentages of Epcam and Vimentin positive HLO on HLO (black bar), sHLO (red bar) and cHLO (blue bar) populations. Results represent mean ±s.d., n=8-20 organoids. J. 20-30 HLO were cultured in the presence or absence of oleic acid (800 μM) for 5 days. P3NP was measured by ELISA with those supernatants. The final values were normalized by the exact number of organoids in each well. P3NP was 2.8 fold increased in 800 μM OA treatment (blue bar), when compared with non-treatment (black bar).

[0010] FIG 3. Cirrhotic transition of steatohepatitis HLO measured by AFM. A. Schematic representation for measuring the stiffness of HLO by AFM. The top region of each single HLO (14×14 matrix in a 25×25 μm square) was scanned with an AFM cantilever, which can provide a spatial mapping of topographical and mechanical information of HLO. Scale bar, 100 μm. B. The representative histogram of calculated Young's modulus (stiffness of HLO; E, kPa) of single HLO showed Gaussian-like distribution and its peak values and width were increased in a dose depended manner 0 (black), 200 (red), 400 (green) and 800 (blue) μM OA. C. Young's modulus (stiffness of HLO) was determined from 7-12 organoids and summarized by the dot plot with box-and-whisker plot. Increase of the median value was observed in a dose dependent manner 0 (black), 200 (red), 400 (green) and 800 (blue) μM OA.

[0011] FIG 4. cHLO rigidity recapitulates clinical phenotype of Wolman disease A. Bright-field image of HLO and cHLO established from several iPSC lines including heathy person (317D6), NAFLD patients (NAFLD150, NAFLD77, and NAFLD27), and the Wolman disease patients (WD90, WD92, and WD91). B.

Young's modulus (stiffness of HLO: Pa) of average of single HLO and cLO derived from several iPSC lines.

[0012] FIG 5. Modeling human phenotypic variation of steatosis using iPSC-sHLO A. Representative allelic functions of PNPLA3, GCKR, and TM6SF2 responsible for hepatic TG content increase. B. Pie chart showing percent distribution of publicly available 2504 cell lines based on total polygenic scoring of three risk allele: 0.6<x (green area), 0.3<x<=0.6 (yellow area), x<=0.3 (brown area). C. The table summarizes the donor characteristic including polygenic score assigned in further study. D. Live-cell imaging of lipid droplets (green) and nuclear (blue) on three group of total polygenic scoring of three allele: 0.6<x, 0.3<x<=0.6, x<=0.3. The image was adopted from the overlay of 10-20 Z-stack images. E. Representative total lipid volume normalized by each organoid size on three group of total polygenic scoring of three allele: 0.6<x, 0.3<x<=0.6, x<=0.3. Red and navy bar indicates 800 μM OA and 200 μM OA treated sHLO, respectively. F. Representative gene expression of pro-inflammatory cytokines on three group of total polygenic scoring of three allele: 0.6<x (black bar), 0.3<x<=0.6 (red bar), x<=0.3 (blue bar). G. Young's modulus (stiffness of HLO: Pa) of average of single cLO on three group of total polygenic scoring of three allele: 0.6<x (black dots), 0.3<x<=0.6 (red dots), x<=0.3 (blue dots). H. OCA response

[0013] FIG 6. Phagocyte activity on THP-1

[0014] FIG 7. Lipids accumulation comparison of 800 μM of OA, PA, LA, and SA.

[0015] FIG 8. Actual migration cell number of THP-1 by 400 and 800 μM of OA

[0016] FIG 9. A. Photo of E-cad positive and negative sorted reconstituted spheroids from E-cad-mruby organoids, HepG2, LX-2, and THP-1. B. Gene expression of pro-inflammatory cytokines TNF-alpha and IL-8. C. ELISA measurement of P3NP.

[0017] FIG 10. No effectiveness of resveratrol on ROS production of liver organoids

[0018] FIG 11. Percentages of BODIPY positive cells (lipids) were determined by flow cytometry. Results represent mean ±s.d., n=5.

[0019] FIG 12. Lipids accumulation in the organoid in the presence and absence of 400 μM Intralipid

[0020] FIG 13. Bright-field image of liver organoids in the culture of non-treatment, 800 μM of OA alone, and 800 μM of OA with 40ng/ml FGF19.

Detailed Description of the Invention

[0021] Unless otherwise noted, terms are to be understood according to conventional usage by those of ordinary skill in the relevant art.

[0022] The term "about" or "approximately" means within an acceptable error range for the particular value as determined by one of ordinary skill in the art, which will depend in part on how the value is measured or determined, e.g., the limitations of the measurement system. For example, "about" can mean within 1 or more than 1 standard deviation, per the practice in the art. Alternatively, "about" can mean a range of up to 20%, or up to 10%, or up to 5%, or up to 1% of a given value. Alternatively, particularly with respect to biological systems or processes, the term can mean within an order of magnitude, preferably within 5-fold, and more preferably within 2-fold, of a value. Where

particular values are described in the application and claims, unless otherwise stated the term "about" meaning within an acceptable error range for the particular value should be assumed.

[0023] As used herein, the term "totipotent stem cells" (also known as omnipotent stem cells) are stem cells that can differentiate into embryonic and extra-embryonic cell types. Such cells can construct a complete, viable organism. These cells are produced from the fusion of an egg and sperm cell. Cells produced by the first few divisions of the fertilized egg are also totipotent.

[0024] As used herein, the term "pluripotent stem cells (PSCs)" encompasses any cells that can differentiate into nearly all cell types of the body, i.e., cells derived from any of the three germ layers (germinal epithelium), including endoderm (interior stomach lining, gastrointestinal tract, the lungs), mesoderm (muscle, bone, blood, urogenital), and ectoderm (epidermal tissues and nervous system). PSCs can be the descendants of inner cell mass cells of the preimplantation blastocyst or obtained through induction of a non-pluripotent cell, such as an adult somatic cell, by forcing the expression of certain genes. Pluripotent stem cells can be derived from any suitable source. Examples of sources of pluripotent stem cells include mammalian sources, including human, rodent, porcine, and bovine.

[0025] As used herein, the term "induced pluripotent stem cells (iPSCs)," also commonly abbreviated as iPS cells, refers to a type of pluripotent stem cells artificially derived from a normally non-pluripotent cell, such as an adult somatic cell, by inducing a "forced" expression of certain genes. hiPSC refers to human iPSCs.

[0026] As used herein, the term "embryonic stem cells (ESCs)," also commonly abbreviated as ES cells, refers to cells that are pluripotent and derived from the inner cell mass of the blastocyst, an early-stage embryo. For purpose of the present invention, the term "ESCs" is used broadly sometimes to encompass the embryonic germ cells as well.

[0027] As used herein, the term "precursor cell" encompasses any cells that can be used in methods described herein, through which one or more precursor cells acquire the ability to renew itself or differentiate into one or more specialized cell types. In some embodiments, a precursor cell is pluripotent or has the capacity to becoming pluripotent. In some embodiments, the precursor cells are subjected to the treatment of external factors (e.g., growth factors) to acquire pluripotency. In some embodiments, a precursor cell can be a totipotent (or omnipotent) stem cell; a pluripotent stem cell (induced or non-induced); a multipotent stem cell; an oligopotent stem cells and a unipotent stem cell. In some embodiments, a precursor cell can be from an embryo, an infant, a child, or an adult. In some embodiments, a precursor cell can be a somatic cell subject to treatment such that pluripotency is conferred via genetic manipulation or protein/peptide treatment.

[0028] Pluripotent Stem Cells Derived from Embryonic Cells.

[0029] In some embodiments, one step is to obtain stem cells that are pluripotent or can be induced to become pluripotent. In some embodiments, pluripotent stem cells are derived from embryonic stem cells, which are in turn derived from totipotent cells of the early mammalian embryo and are capable of unlimited, undifferentiated proliferation in vitro. Embryonic stem cells are pluripotent stem cells derived from the inner cell mass of the

blastocyst, an early-stage embryo. Methods for deriving embryonic stem cells from blastocytes are well known in the art. Human embryonic stem cells H9 (H9-hESCs) are used in the exemplary embodiments described in the present application, but it would be understood by one of skill in the art that the methods and systems described herein are applicable to any stem cells.

[0030] Additional stem cells that can be used in embodiments in accordance with the present invention include but are not limited to those provided by or described in the database hosted by the National Stem Cell Bank (NSCB), Human Embryonic Stem Cell Research Center at the University of California, San Francisco (UCSF); WISC cell Bank at the Wi Cell Research Institute; the University of Wisconsin Stem Cell and Regenerative Medicine Center (UW-SCRMC); Novocell, Inc. (San Diego, Calif.); Cellartis AB (Goteborg, Sweden); ES Cell International Pte Ltd (Singapore); Technion at the Israel Institute of Technology (Haifa, Israel); and the Stem Cell Database hosted by Princeton University and the University of Pennsylvania. Exemplary embryonic stem cells that can be used in embodiments in accordance with the present invention include but are not limited to SA01 (SA001); SA02 (SA002); ES01 (HES-1); ES02 (HES-2); ES03 (HES-3); ES04 (HES-4); ES05 (HES-5); ES06 (HES-6); BG01 (BGN-01); BG02 (BGN-02); BG03 (BGN-03); TE03 (13); TE04 (14); TE06 (16); UC01 (HSF1); UC06 (HSF6); WA01 (H1); WA07 (H7); WA09 (H9); WA13 (H13); WA14 (H14).

[0031] More details on embryonic stem cells can be found in, for example, Thomson et al., 1998, "Embryonic Stem Cell Lines Derived from Human Blastocysts," Science 282 (5391):1145-1147; Andrews et al., 2005, "Embryonic stem (ES) cells and

embryonal carcinoma (EC) cells: opposite sides of the same coin," Biochem Soc Trans 33:1526-1530; Martin 1980, "Teratocarcinomas and mammalian embryogenesis,". Science 209 (4458):768-776; Evans and Kaufman, 1981, "Establishment in culture of pluripotent cells from mouse embryos," Nature 292(5819): 154-156; Klimanskaya et al., 2005, "Human embryonic stem cells derived without feeder cells," Lancet 365 (9471): 1636-1641; each of which is hereby incorporated herein in its entirety.

[0032] Induced Pluripotent Stem Cells (iPSCs)

[0033] In some embodiments, iPSCs are derived by transfection of certain stem cell-associated genes into non-pluripotent cells, such as adult fibroblasts. Transfection is typically achieved through viral vectors, such as retroviruses. Transfected genes include the master transcriptional regulators Oct-3/4 (Pouf51) and Sox2, although it is suggested that other genes enhance the efficiency of induction. After 3-4 weeks, small numbers of transfected cells begin to become morphologically and biochemically similar to pluripotent stem cells, and are typically isolated through morphological selection, doubling time, or through a reporter gene and antibiotic selection. As used herein, iPSCs include but are not limited to first generation iPSCs, second generation iPSCs in mice, and human induced pluripotent stem cells. In some embodiments, a retroviral system is used to transform human fibroblasts intopluripotent stem cells using four pivotal genes: Oct3/4, Sox2, Klf4, and c-Myc. In alternative embodiments, a lentiviral system is used to transform somatic cells with OCT4, SOX2, NANOG, and LIN28. Genes whose expression are induced in iPSCs include but are not limited to Oct-3/4 (e.g., Pou5fl); certain members of the Sox gene family (e.g., Sox1,

Sox2, Sox3, and Sox15); certain members of the Klf family (e.g., Klf1, Klf2, Klf4, and Klf5), certain members of the Myc family (e.g., C-myc, L-myc, and N-myc), Nanog, and LIN28.

[0034] In some embodiments, non-viral based technologies are employed to generate iPSCs. In some embodiments, an adenovirus can be used to transport the requisite four genes into the DNA of skin and liver cells of mice, resulting in cells identical to embryonic stem cells. Since the adenovirus does not combine any of its own genes with the targeted host, the danger of creating tumors is eliminated. In some embodiments, reprogramming can be accomplished via plasmid without any virus transfection system at all, although at very low efficiencies. In other embodiments, direct delivery of proteins is used to generate iPSCs, thus eliminating the need for viruses or genetic modification. In some embodiment, generation of mouse iPSCs is possible using a similar methodology: a repeated treatment of the cells with certain proteins channeled into the cells via poly-arginine anchors was sufficient to induce pluripotency. In some embodiments, the expression of pluripotency induction genes can also be increased by treating somatic cellswith FGF2 under low oxygen conditions.

[0035] More details on embryonic stem cells can be found in, for example, Kaji et al., 2009, "Virus free induction of pluripotency and subsequent excision of reprogramming factors," Nature 458:771-775; Woltjen et al., 2009, "piggyBac transposition reprograms fibroblasts to induced pluripotent stem cells," Nature 458:766-770; Okita et al., 2008, "Generation of Mouse Induced Pluripotent Stem Cells Without Viral Vectors," Science 322(5903):949-953; Stadtfeld et al., 2008, "Induced Pluripotent Stem Cells Generated without Viral Integration," Science

322(5903):945-949; and Zhou et al., 2009, "Generation of Induced Pluripotent Stem Cells Using Recombinant Proteins," Cell Stem Cell 4(5):381-384; each of which is hereby incorporated herein in its entirety.

[0036] In some embodiments, exemplary iPS cell lines include but not limited to iPS-DF19-9; iPS-DF19-9; iPS-DF4-3; iPS-DF6-9; iPS(Foreskin); iPS(IMR90); and iPS(IMR90).

[0037] More details on the functions of signaling pathways relating to DE development can be found in, for example, Zorn and Wells, 2009, "Vertebrate endoderm development and organ formation," Annu Rev Cell Dev Biol 25:221-251; Dessimoz et al., 2006, "FGF signaling is necessary for establishing gut tube domains along the anterior-posterior axis in vivo," Mech Dev 123:42-55; McLin et al., 2007, "Repression of Wnt/β-catenin signaling in the anterior endoderm is essential for liver and pancreas development. Development," 134:2207-2217; Wells and Melton, 2000, Development 127:1563-1572; de Santa Barbara et al., 2003, "Development and differentiation of the intestinal epithelium," Cell Mol Life Sci 60(7): 1322-1332; each of which is hereby incorporated herein in its entirety.

[0038] Any method for producing definitive endoderm from pluripotent cells (e.g., iPSCs or ESCs) are applicable to the methods described herein. Exemplary methods are disclosed in, for example, "Methods and systems for converting precursor cells into intestinal tissues through directed differentiation," US9719068B2 to Wells et al., and "Methods and systems for converting precursor cells into gastric tissues through directed differentiation," US20170240866A1, to Wells et al. In some embodiments, pluripotent cells may be derived from a morula. In some embodiments, pluripotent stem cells may be stem cells.

Stem cells used in these methods can include, but are not limited to, embryonic stem cells. Embryonic stem cells may be derived from the embryonic inner cell mass or from the embryonic gonadal ridges. Embryonic stem cells or germ cells can originate from a variety of animal species including, but not limited to, various mammalian species including humans. In some embodiments, human embryonic stem cells are used to produce definitive endoderm. In some embodiments, human embryonic germ cells are used to produce definitive endoderm. In some embodiments, iPSCs are used to produce definitive endoderm. Additional methods for obtaining or creating DE cells that can be used in the present invention include but are not limited to those described in United States Patent No. 7,510,876 to D'Amour et al.; United States Patent No. 7,326,572 to Fisk et al.; Kubo1 et al., 2004, "Development of definitive endoderm from embryonic stem cells in culture," Development 131:1651-1662; D'Amour et al., 2005, "Efficient differentiation of human embryonic stem cells to definitive endoderm," Nature Biotechnology 23:1534-1541; and Ang et al., 1993, "The formation and maintenance of the definitive endoderm lineage in the mouse: involvement of HNF3/forkhead proteins," Development 119:1301-1315.

[0039] Non-alcoholic Fatty Liver Disease (NAFLD) is one of the major challenges to be overcome in developed countries to do the increased chance of developing lethal liver disorders, yet effective treatment is lacking. Similarly, iatrogenic parental nutrition associated liver disease (PNALD) is a disorder that currently has no effective treatment. Models having steatohepatitis and/or clinical histopathological features of liver disease such as lipid droplet accumulation and cystoskeleton filament disorganization, steatosis, and hepatocellular ballooning are needed. Despite the promise of disease models using patients'

stem cells, current approaches are limited in their applications to unicellular, monogenic and relatively simple pathologies, failing to capture more prevailing and complex disease pathology such as epithelial organ fibrosis.

[0040] In one aspect, a method of making a lipotoxic organoid model is disclosed. The method may comprise the steps of contacting a liver organoid made according to the methods described herein, with a free fatty acid (FFA) composition. The FFA composition may comprise oleic acid, linoleic acid, palmitic acid, or combinations thereof, preferably oleic acid. The amount of FFA may be determined by one of ordinary skill in the art. In one aspect, the FFA, preferably oleic acid, may be contacted with a liver organoid in an amount of from about 10 μM to about 10,000 μM, or from about 20 μM to about 5,000 μM, or from about 30 μM to about 2500 μM, or from about 40 μM to about 1250 μM or from about 50 μM to about 1000 μM, or from about 75 μM to about 900 μM or from about 80 μM to about 800 μM, or from about 90 μM to about 700 μM, or about 100 μM to about 500 μM, or from about 200 μM to about 400 μM. The FFA may be contacted with the liver organoid for a period of time of from about 1 hour to about 10 days, or from about 2 hours to about 9 days, or from about 3 hours to about 8 days, or from about 4 hours to about 7 days, or from about 5 hours to about 6 days, or from about 6 hours to about 5 days, or from about 7 hours to about 4 days, or from about 8 hours to about 3 days, or from about 9 hours to about 2 days, or from about 10 hours to about 1 day. In one aspect, the range is about 3 to about 5 days, +/- 24 hours.

[0041] In one aspect, the lipotoxic organoid model is a model of fatty liver disease.

[0042] In one aspect, the lipotoxic organoid model is a model of steatohepatitis.

[0043] In one aspect, the lipotoxic organoid model is a model of cirrhosis.

[0044] In one aspect, the lipotoxic organoid model is a model of parenteral nutrition associated liver disease (PNALD).

[0045] In one aspect, the lipotoxic organoid model is a model of NAFLD.

[0046] In one aspect, the lipotoxic organoid model may be characterized by cytoskeleton filament disorganization, ROS increase, mitochondrial swelling, trigycleride accumulation, fibrosis, hepatocyte ballooning, IL6 secretion, steatosis, inflammation, ballooning and Mallory's body-like, tissue stiffening, cell-death, and combinations thereof.

[0047] In one aspect, a method of screening for a drug for treatment of a liver disease, including NAFLD and/or cholestasis is disclosed. The method may comprise the step of contacting a candidate drug with a lipotoxic organoid model as disclosed herein.

[0048] In one aspect, a method of assaying the effectiveness of a nutritional supplement/TPN is disclosed. The method may comprise the step of contacting the nutritional supplement/TPN with a lipotoxic organoid model as disclosed herein.

[0049] In one aspect, the three-dimensional (3D) liver organoid model of fatty liver disease is disclosed, wherein the organoid is characterized by steatosis, inflammation, ballooning and Mallory's bodies, ROS accumulation and mitochondrial overload; fibrosis and tissue stiffening, and cell death.

[0050] In one aspect, the three-dimensional (3D) liver organoid model is a model of drug induced hepatotoxicity and inflammation/fibrosis.

[0051] In one aspect, the three-dimensional (3D) liver organoid model is a model of parenteral nutrition associated liver disease (PNALD)

[0052] In one aspect, the three-dimensional (3D) liver organoid model does not comprise inflammatory cells, for example T-cells or other inflammatory secreted proteins.

[0053] Also disclosed are methods of inducing formation of a liver organoid from iPSC cells which may be used in the aforementioned methods and/or to obtain the aforementioned compositions. The method may comprise the steps of

[0054] a) contacting definitive endoderm (DE) derived from iPSC cells with a FGF pathway activator and a GSK3 inhibitor, for a period of time sufficient to form posterior foregut spheroids, preferably for a period of time of from about 1 day to about 3 days and b) incubating the resulting posterior foregut spheroids of step a in the presence of retinoic acid (RA) for a period of time sufficient to form a liver organoid, preferably for a period of time of from about 1 to about 5 days, preferably about 4 days.

[0055] Fibroblast growth factors (FGFs) are a family of growth factors involved in angiogenesis, wound healing, and embryonic development. The FGFs are heparin-binding proteins and interactions with cell-surface associated heparan sulfate proteoglycans have been shown to be essential for FGF signal transduction. Suitable FGF pathway activators will be readily understood by one of ordinary skill in the art. Exemplary FGF pathway activators include, but are not limited to: one or more molecules selected from the group consisting of FGF1, FGF2,

FGF3, FGF4, FGF10, FGF11, FGF12, FGF13, FGF14, FGF15, FGF16, FGF17, FGF18, FGF19, FGF20, FGF21, FGF22, and FGF23. In some embodiments, siRNA and/or shRNA targeting cellular constituents associated with the FGF signaling pathway may be used to activate these pathways.

[0056] In some embodiments, DE culture is treated with the one or more molecules of a signaling pathway described herein at a concentration of 10 ng/ml or higher; 20 ng/ml or higher; 50 ng/ml or higher; 75 ng/ml or higher; 100 ng/ml or higher; 120 ng/ml or higher; 150 ng/ml or higher; 200 ng/ml or higher; 500 ng/ml or higher; 1,000 ng/ml or higher; 1,200 ng/ml or higher; 1,500 ng/ml or higher; 2,000 ng/ml or higher; 5,000 ng/ml or higher; 7,000 ng/ml or higher; 10,000 ng/ml or higher; or 15,000 ng/ml or higher. In some embodiments, concentration of signaling molecule is maintained at a constant throughout the treatment. In other embodiments, concentration of the molecules of a signaling pathway is varied during the course of the treatment. In some embodiments, a signaling molecule in accordance with the present invention is suspended in media comprising DMEM and fetal bovine serine (FBS). The FBS can be at a concentration of 2% and more; 5% and more; 10% or more; 15% or more; 20% or more; 30% or more; or 50% or more. One of skill in the art would understand that the regiment described herein is applicable to any known molecules of the signaling pathways described herein, alone or in combination, including but not limited to any molecules in the FGF signaling pathway.

[0057] Suitable GSK3 inhibitors will be readily understood by one of ordinary skill in the art. Exemplary GSK3 inhibitors include, but are not limited to: Chiron/ CHIR99021, for example, which inhibits GSK3β. One of ordinary skill in the art will recognize

GSK3 inhibitors suitable for carrying out the disclosed methods. The GSK3 inhibitor may be administered in an amount of from about 1 uM to about 100 uM, or from about 2 uM to about 50 uM, or from about 3 uM to about 25 uM. One of ordinary skill in the art will readily appreciate the appropriate amount and duration.

[0058] In one aspect, the stem cells may be mammalian, or human, iPSCs.

[0059] In one aspect, the foregut spheroids may be embedded in a basement membrane matrix, such as, for example, the commercially available basement membrane matrix sold under the tradename Matrigel.

[0060] In one aspect, the liver organoids may be characterized in that the liver organoids may express alpha-fetoprotein (AFP), albumin (ALB), retinol binding protein (RBP4), cytokeratin 19 (CK19), hepatocyte nuclear factor 6 (HNF6), and cytochrome P450 3A4 (CYP3A4), HNF4a, E-cadherin, DAPI, and Epcam. Such expression may occur, for example, at day 40 to day 50. The expression level may be similar to that observed in human liver cells, for example, that of an adult liver cell.

[0061] In one aspect, the liver organoid may be characterized in that the liver organoid has bile transport activity.

[0062] In one aspect, the liver organoid may be derived from a stem cell and may comprise a luminal structure further containing internalized microvilli and mesenchymal cells. The luminal structure may be surrounded by polarized hepatocytes and a basement membrane. The liver organoid may comprise functional stellate cells and functional Kupffer cells.

[0063] The liver organoid may, in certain aspects, be characterized by having one or more of the following: bile production capacity, bile transport activity, Complement factor H expression of at least 50 ng/mL/1xe^6 cells/24hr, Complement factor B of at least 40 ng/mL/1xe^{6}cells/24hr, C3 expression of at least 1000 ng/mL/1xe^{6}cells/24hr; C4 expression of at least 1000 ng/mL/1xe^{6}cells/24hr, fibrinogen production of at least 1,000 ng/mL/1xe^{6}cells/24hr and albumin production of at least 1,000 ng/mL/1xe^{6}cells/24hr. In one aspect, the liver organoid may be characterized by having total hepatic protein expression of at least 10,000 ng/mL 1xe^{6}cells/24 hours. The liver organoid may be characterized in that it may express one or more genes selected from PROX1, RBP4, CYP2C9, CYP3A4, ABCC11, CFH, C3, C5, ALB, FBG, MRP2, ALCAM, CD68, CD34, CD31. In one aspect, the liver organoid may comprise cells comprising a drug metabolism cytochrome variant, such as, for example, a CY2C9*2 variant. The liver organoid may comprise a vasculature, such as that described in US 20160177270.

[0064] In one aspect, the liver organoid may be characterized in that the liver organoid does not comprise inflammatory cells, for example T-cells or other inflammatory secreted proteins.

[0065] Examples

[0066] Human organoid systems that achieved the higher-order function of 3D tissues closely resemble *in vivo* organ architecture in health and disease, yet failed to capture more prevailing and complex pathology such as inflammation and fibrosis. Here, Applicant developed multi-cellular human liver organoid (HLO) model that displays essential features of steatohepatitis. Cultural fatty acid exposure enables persistent steatosis induction, followed by progressive activation of pro-inflammatory and fibrotic lineages

that develops massive fibrosis in HLO. Interestingly, expression of the steatohepatitis phenotype is strongly influenced by clinically reported heritable factors. Atomic force microscopy measurement revealed that overall organoid stiffening correlates the severity of inflammation and fibrosis. The measurement fidelity to clinical phenotype was confirmed using three monogenic steatohepatitis-specific iPSC lines. Furthermore, Applicant established an iatrogenic parental nutrition associated liver disease (PNALD) model in organoids.

[0067] Retinoic acid (RA) signaling is a well-known important specifier of thyroid, lung, and pancreas from foregut endoderm during the early organ specification phase, whereas it is clearly not essential for specification of the liver in model organisms (Kelly and Drysdale, 2015) with the exception of zebrafish (Negishi et al., 2010). Indeed, xenopus and chick are similar to mammals as liver specification occurs in embryos lacking RA (Chen et al., 2004; Stafford et al., 2004). Conversely, several animal studies suggested that RA promotes hepatic stellate cell differentiation from mesenchyme, which is controlled in part by the zinc finger transcription factor WT1 expressed in the STM and stellate cells (Ijpenberg et al., 2007; Wang et al., 2013). Additionally, several studies suggest that the balanced RA regulation induces monocyte fate specification from human stem cells (Purton et al., 2000; Ronn et al., 2015). Also, later liver bud growth is promoted by RA signaling via unknown mechanisms (Zorn and Wells, 2009). Given the broader roles of RA for both parenchymal and non-parenchymal cell specification, Applicant hypothesized that the timed RA exposure might impact lineage diversification of hepatic stromal cells including pro-inflammatory lineages, thereby facilitating creation of human liver organoids for modeling inflammation and fibrosis.

[0068] Recently, directed differentiation into intestinal organoids via foregut spheroid generation from PSC has been reported (McCracken et al., 2017; Spence et al., 2011). These organoids do not merely generate epithelial cells but also co-develop mesenchymal cell components. Here, by taking advantage of this foregut generation method, Applicant tested the hypothesis that the timely RA pulsing into liver organoids preferentially co-differentiates supportive lineages after hepatic specification from human iPSC. By fostering close interactions between epithelial and supportive lineages in a 4-D condition wherein they can co-develop, Applicant demonstrated the applicability of the liver organoid to model inflammation and fibrosis. Applicant also established a screen platform to determine the severity of fibrosis by evaluating stiffness at single organoid level in the living state. This method serves as an invaluable application platform for the study of epithelial organ inflammation and fibrosis towards drug development and personalized therapy.

[0069] **RESULTS**

[0070] **Generation of RA-based liver organoid model from human iPSCs**

[0071] To elucidate whether RA signaling has an impact on determining the lineage differentiation towards stromal cells, Applicant established a liver organoid model from human iPSCs by transient induction of RA. Applicant initially differentiated iPSCs to foregut spheroids through definitive endoderm (DE) specification as previously described (Spence et al., 2011). The foregut spheroids were mixed with the attached cells grown in the same well, and the mixture was embedded in Matrigel. Since RA is a known specifier for diverse lineages through a context dependent process, Applicant set the duration of initial RA

signaling before the hepatocyte maturation process which is cultured in hepatocyte culture media (HCM) and characterized the established organoids at day 20 as illustrated in FIG 1, A. Since the highest concentration of albumin in culture media was observed with 4 days of RA exposure among the various duration of RA from 0 to 5 days, the further characterization of the established organoids was compared between two conditions of 0 and 4 days-RA exposure. The number of organoids was increased 1.8-fold in RA treated wells compared to untreated and the size was increased 1.5-fold after RA treatment (FIG 1, B, C, and D). Albumin secretion was increased two-fold in the RA treated group (3.0-6.5 μg/ml) when compared with untreated (0.5-3.5 μg/ml; FIG 1, E). Of note, albumin secretion was maintained more than 40 days after day 20 when albumin was first detected (data not shown). Interestingly, the internal luminal structure appeared in 95% of RA treated organoids, whereas it was detected in only 12% of untreated organoids, indicating that the lumenization of the organoid is dependent on RA signaling (FIG 1, F).

[0072] Applicant next tested the bile transport activity by adding fluorescein diacetate, a marker of efflux transport in hepatocytes which turns into fluorescein after estrase hydrolysis in hepatocytes, into the culture media and tracked the flow of the fluorescence. The fluorescent substance was absorbed into the cells of organoids within minutes after fluorescein diacetate addition and subsequently excreted from the cells into the internal lumen (FIG 1, G). By contrast, the fluorescence was not detected in spheroids. Since bile transport activity is an important function of the liver, human liver organoids, hereafter defined as HLO, may be used as models that represent multiple human

hepatocyte functions including albumin secretion and bile transport functions.

[0073] Co-differentiation of pre-fibrotic and inflammatory lineages in human iPSC-liver organoid

[0074] Interestingly, single-cell RNA sequencing (scRNA-seq) analysis of RA treated HLO showed the expression signatures specific to stellate cells, liver resident macrophage Kupffer cells, and endothelial cells as evidenced by stellate cell markers (ACTA2, DES, PDGFRB), Kupffer cell markers (CD68, IRF7), and endothelial cell markers (OIT3, DPP4, C1QTNF1; FIG 1, H) (Bahar Halpern et al., 2017; El Taghdouini et al., 2015; van de Garde et al., 2016). To confirm the presence of stellate cells and Kupffer cells, Applicant conducted a quantitative analysis by FACS with epithelial cell marker EpCAM, stellate cell marker CD166/ALCAM, and Kupffer cell marker CD68 and F4/80 (Yanagimachi et al., 2013). While the frequency of EpCAM+ cells was 78.85 ±7.35% of HLO, EpCAM-CD166+, EpCAM-CD68+, and EpCAM-F4/80+ expressing cells was 32.4 ±1.2%, 1.69±0.3%, and 1.68±0.2%, respectively (FIG1, I). Upon immunohistochemistry, the expression of CD68 cells was also detected in HLO, and CD68 expression was localized to the cells of the internal lumen side (FIG. 1, J). Vimentin and GFAP, novel markers for human hepatic stellate cells and reported to be required for the process of stellate cell trans-differentiation in rodents (Geerts et al., 2001; Kordes et al., 2014), were both detected in HLO and were co-expressing in the same cells (FIG . 1, J), indicating that stellate cells are resident in HLO.

[0075] To examine whether CD68 expressing cells are functionally active in HLO similar to Kupffer cells, Applicant monitored the phagocytic activity in HLO, which has been reported to be active

in liver resident Kupffer cells, with a pH-sensitive rhodamine-based live-cell dye that undergoes a dramatic increase in fluorescence (red) in response to an environmental shift from high to low pH which occurs in phagocytosis as was observed in THP1 human macrophage cells (FIG 8). In HLO, the activity was detected and localized similar to CD68 expressing cells, whereas it was rarely detected in the spheroid (FIG 1, K). These observations indicate that RA-based liver organoid (HLO) is a unique liver model that naturally develops multi-lineage liver stromal cells including stellate cells and Kupffer cells from human iPSC.

[0076] Inflammation response and fibrosis induction of HLO by free fatty acid

[0077] Currently, free fatty acids (FFA) are widely used as an initiating factor to establish an *in vitro* lipotoxic hepatocyte model; however, fat accumulation is the only phenotype (Kanuri and Bergheim, 2013). Alternate co-culture models of hepatocyte and Kupffer cells showed inflammatory responses such as the increased expression of IL family cytokines, macrophage related cytokines, and MMP related cytokines but not subsequent fibrosis (Hassan et al., 2014). Given the presence of hepatocyte-, stellate- and Kupffer-like cells with lipid metabolism function-associated genes indicated by global transcriptome analysis, Applicant hypothesized that FFA exposure naturally triggers an inflammation response and resulting fibrotic response in HLO. To test this hypothesis, Applicant treated HLO for 3 to 5 days with FFA. Applicant indicated 3 day and 5 days OA treated HLO as steatohepatitis (s)HLO and cirrhosis (c)HLO (FIG. 4, A). sHLO is HLO treated with oleic acid for three days and show lipid accumulation and inflammation. cHLO is HLO treated with

oleic acid for five days and shows fibrosis (HLO is stiffened) in addition to lipid accumulation and inflammation. To first compare the effect of multiple FFAs including oleic acid (OA, 18:1 n9), linoleic acid (LA, 18:2), palmitic acid (PA, 16:0), and stearic acid (SA, 18:0) on lipids accumulation, live-cell imaging was performed with lipid dye BODIPY at 3 days after the FFA exposure. As FIG 7 shows, OA was the most effective in inducing lipid accumulation in hepatocyte like cells, and SA was the least effective. Considering that OA triggers massive lipid accumulation, the concentration of OA was varied (0, 200, 400, and 800 μM) to trigger inflammatory reaction in sHLO. Live-cell imaging and subsequent quantitation displayed that lipid accumulation was elevated in sHLO in a dose dependent fashion (up to 18-fold; FIG. 4, B and C). In addition to increase in lipid accumulation, the size of lipid droplets was enlarged (FIG. 4, B). Hepatocyte ballooning (enlargement) was one of the pathological grading indicators to determine the nonalcoholic steatohepatitis (NASH) activity (NAS scoring), which was confirmed in 800 μM OA treated sHLO by live imaging of cellular membrane (FIG. , 4B). Triglycerides, a main constituent of lipids accumulated in the liver, were also detected in 800 μM treated sHLO, but not in untreated sHLO (FIG.4, D). More importantly, ELISA of culture supernatant showed that IL-6 was secreted 2.2-fold in 800 μM OA treated sHLO culture media when compared to the untreated (FIG. 4, E). IL-8 and TNF-alpha were also upregulated in a 200μM or 800μM OA treated condition (10- and 2-fold increase, respectively; FIG. 4, F). Moreover, using the OA-treated sHLO conditioned media, the migration of THP1 was assessed in 24hrs after culturing in transwells, and THP-1 migration cells were elevated in a OA treated sHLO, suggesting FFA treatment naturally evoked an inflammatory response in sHLO presumably

by causing stress on hepatocyte like cells (up to 2-fold: FIG. 4, G and FIG 8.) To confirm whether those inflammation and fibrosis features were specific to HLO, Applicant isolated epithelial marker E-cad from E-cad mRuby embryonic stem (ES) cells derived organoids, reconstructed the spheroids from either E-cad positive or negative cells, and applied for ELISA for IL6 and P3NP and RNA expression for IL8 and TNF-alpha. As FIG 9 indicates, neither E-cad positive nor negative cells derived spheroids produced P3NP and IL-6 secreted production and overexpressed the gene expression of inflammatory markers. Applicant also tested same experiments using human hepatocyte cell line HepG2, Macrophage cell line THP-1, and hepatic stellate cell LX-2, and had a similar result of E-cad positive and negative cells. The results demonstrated that liver organoids only response to FFA treatment on inflammation and fibrosis response.

[0078] To further determine whether HLO progresses towards fibrosis-like condition, Applicant performed Masson trichrome stain on sHLO and cHLO. Trichrome positive HLO was not observed on sHLO but significantly increased on cHLO (FIG. 2, H). Moreover, IF staining of epithelial marker Epcam and fibrosis marker Vimentin demonstrated increase of Epcam positive HLO and decrease of vimentin positive HLO in cHLO (FIG. 2, I), suggesting that OA treatment induced the selective increase in fibrotic population as well as matrix deposition in cHLO. Moreover, ELISA of P3NP was also measured at day 5 of OA exposure. P3NP secretion was increased 2.8-fold in the culture media of 800 μM OA treated HLO when compared with the untreated (FIG.4, J). Collectively, these observations indicated that FFA exposure not merely caused an accumulation of

triglycerides but also initiated an inflammatory reaction and fibrosis in HLO.

[0079] cHLO profile of inflammation and fibrosis by FFA treatment at single cell level

[0080] High-throughput quantification of fibrosis by AFM

[0081] Accumulating evidence has indicated that liver stiffness is well correlated with the severity of liver fibrosis (Yoneda et al., 2008) and thereby measuring the stiffness of HLO has potential to evaluate the fibrosis severity of HLO. Applicant's preliminary qualitative analysis of smooth muscle actin immunostaining indicates dose dependent fibrosis progression by OA exposure (FIG. 2, H, I, and J). To gain more quantitative insights in a screenable format, Applicant thus assessed in the living state whether HLO fibrosis could increase the stiffness in a dose dependent fashion using micro-indentation with Atomic Force Microscopy (AFM). As shown in FIG. 4, A, the top region of each single HLO (14×14 matrix in a 25×25 μm square) was scanned with an AFM cantilever, which can provide a spatial mapping of topographical and mechanical information of HLO. The representative histogram of calculated Young's modulus (E, kPa) of single HLO clearly showed a Gaussian-like distribution and its peak values and width were increased in accordance with the OA concentration (FIG.4, B; 0, 200, 400, 800 μM). Young's moduli determined from HLOs were summarized by dot plot with box-and-whisker plot (FIG. 4, C), demonstrating that the rigidity of HLO was gradually elevated from 0 to 800 μM OA *i.e.*, gradual shift of median value and enlargement of the stiffness range were observed according to the elevation of OA concentration. The Emedian values were 1.2 kPa, 1.6 kPa, 2.4 kPa and 2.8 kPa for 0, 200, 400, and 800 μM OA-treated

organoids, respectively. Furthermore, difference between 90th percentile and 10th percentile (ΔP90-10) was 3.2 kPa for untreated organoids and 7.0 kPa for 800 μM OA-treated organoids was observed. As FIG. 3, F shows, TNF-alpha and IL-8 were also upregulated by OA addition, known to be correlated with fibrosis severity in NAFLD patients (Ajmera et al., 2017). These results indicate that stiffness of HLO can be a quantifiable measurement for the severity of fibrosis, and thus can be potentially applied for a high-throughput screening of fibrosis.

[0082] cHLO rigidity recapitulates clinical phenotype of Wolman disease

[0083] The clinical relevance of a model relating to fibrosis and cirrhosis from pluripotent stem cells is unclear due to the undetermined nature of genetic influences in a patient. A predisposition to fibrosis probably would not be captured in this model. Applicant therefore has examined assay fidelity to clinical phenotype by evaluating congenital steatohepatitis patient derived iPSC including healthy people (317D6), NAFLD/NASH patients (NAFLD150, 77, and 27) and Wolman disease patients (WD90, 91, and 92)(FIG 5, A). Specifically, Applicant established three Wolman disease patient-specific iPSC lines, which is a mono-genetic disorder with lethal steatohepatitis, and confirmed the significant rigidity increase relative to normal iPSC line-derived organoids, notably with remarkable correlation to enzymatic activity at the time of clinical diagnosis (FIG. 5, B).

[0084] Modeling human phenotypic variation of steatosis using iPSC-sHLO.

[0085] Second, Applicant extended this new organoid model to assess the polygenic effects on steatohepatitis progression. Three

protein coding sequencing variants PNPLA3 (patatin-like phospholipase3) p.I148M, TM6SF2 (Transmembrane 6 Superfamily Member 2) p.E167K, and GCKR (Glucokinase regulatory protein) p.P446L which have been repeatedly shown to be independent determinants of hepatic triglyceride content (HTGC) by large-scale GWAS (Xu et al., 2015),(Zain et al., 2015) (FIG. 6, A). Applicant therefore approached large scale cell bank, and mapped out 2504 cell lines with the polygenic score (FIG. 6, B) by a summation of reported effect size β(SNP) (Stender et al., 2017), per-allele change in standardized HTGC multiplying weighted dosage as follow: ∑{β (SNP) x (dosage of risk allele) }. After the acquisition of iPSC lines with three different thresholds (FIG. 6, B and C), Applicant has generated seven iPSC organoids, and induced steatohepatitis to estimate polygenic impacts on the phenotype. Strikingly, Applicant has found the remarkable correlation of 'steatosis' (by live imaging, FIG. 6, D and E) and 'inflammation' (qRT-PCR, FIG. 6, F), but NOT for 'fibrosis' (AFM based stiffness measurements, FIG. 6, G) to polygenic scores. Applicant also found that OCA reponse differ among the cell line and response to OCA are depended on SNP number (FIG, 6H)

[0086] DISCUSSION

[0087] Multi-cellular liver organoid from human PSC

[0088] A series of recent studies reported the successful integration of supportive lineages into endoderm-derived organoids by experimentally combining endothelial cells (Takebe et al., 2013), mesenchymal cells (Takebe et al., 2015), and neural crest cells (Workman et al., 2017). The RA-pulsation based method naturally engages cells to diversify with a sustained cell polarity, and is remarkably reproducible and scalable with reasonable cost.

Whether the precise nature of supportive lineages is developmentally relevant or liver specific remains elusive, the stromal populations are fully reactive to known fibrosis inducers including LPS and fatty acids, paving a new way for modeling multicellular and complex pathologies.

[0089] Promise of mechanical organoid screening for analyzing inflammation and fibrosis

[0090] From a future screening standpoint, single organoid based liver measurement is a highly attractive readout due to its robustness, normalization and relative simplicity. For example, based on live fluorescent imaging analysis of an organoid, a functional swelling assay was established for cystic fibrosis patients' gut organoids, demonstrating an effective drug selection (Saini, 2016). Live rigidity assessment on a single liver organoid from iPSC is an effective way to predict the severity of fibrosis. A significant correlation between liver stiffness measurement and fibrosis stage is clinically reported in fatty liver disease patients by elastography (Yoneda et al., 2008). In addition, a strong association between increased liver stiffness and presence of diabetes mellitus (DM) and/or greater insulin resistance was observed in a subgroup of subjects with ultrasonographically defined NAFLD (Koehler et al., 2016). Interestingly, human liver organoid (HLO) stiffness increased in proportion to both LPS and FFAs, accompanied by inflammatory cytokine production and fibroblast expansion. Considering a number of epithelial organ fibrosis share a similar phenotype via diverse pathological mechanisms, an organoid based rigidity detection assay could be used to analyze fibrosis using lung, kidney, cardiac and gut organoids.

[0091] In liver organoids, multiple measurements can be intra-vitally evaluated with the use of high content imaging system. In fact, increases in the number and size of lipid droplets, bile transport activity, phagocytes, and the deterioration of cellular morphology can be effectively imaged in fat-treated liver organoids. Thus, organoid based assay platforms may be used to better understand the human specific mechanisms of fatty liver diseases and establishing high-content screening for drug discovery for these diseases. Combined with compound libraries and nutritional metabolites, organoid based mechanical screening would be highly attractive model system for implicating effective therapy in humans, otherwise not testable preclinically.

[0092] Nutritional Precision Medicine (Therapy personalization)

[0093] Patient-specific iPSC-derived organoids might be used to predict individualized drug efficacy and epithelial response. Human iPSCs can be established from both healthy and diseased individuals. In parallel to the establishment of a population iPSC panel, the use of patients' iPSCs is expected to model inter-individual differences of lipotoxicity, drug efficacy and safety concerns (Warren et al., 2017a; Warren et al., 2017b). In doing so, phenotypic screening using a liver organoid-based platform will promote personalized selection of highly effective interventions for the disorders. For instance, as the nutritional supplementation might be altered depending on individuals, the disclosed system may be a highly compatible assay for reflecting nutrition associated conditions before administration. Specifically, patient-specific iPSC-derived organoids can be used to customize PN formulation to each patient with the aim of minimizing the possible progression to hepatic steatosis and fibrosis (PNALD). Indeed, in clinics, PN formulation is often

customized (Mercaldi et al., 2012) as commercial solutions do not meet the caloric, amino acid, and electrolyte needs of critically ill patients, who are often obese and require fluid restriction, and display hepatic/renal dysfunction (Boullata et al., 2014). Beyond nutritional needs, there is an urgent need to gain insights for a reduction of possible adverse effects associated with PN products. The liver organoid would thus be useful to evaluate safety concerns especially for PNALD risk assessment, facilitating the customization strategy of PN formulations for each patient.

[0094] Overall, Applicant has demonstrated that enabling crosstalk between epithelial and stromal lineages in a 4-D organoid culture is useful for modeling clinically relevant pathology associated with steatosis and fibrosis of liver. This model will eventually lead to analysis of more prevailing pathology such as NAFLD or NASH, which is a growing concern with population aging. More broadly, Applicant has established a viable strategy for modeling humanistic complex pathology coupled with currently evolving organoid technology (Lancaster and Knoblich, 2014), paving a new way for the discovery of effective treatments against unrecoverable diseases at single organoid level.

[0095] METHODS

[0096] hPSCs Maintenance. The TkDA3 human iPSC clone used in this study was kindly provided by K. Eto and H. Nakauchi. Human iPSC lines were maintained as described previously (Takebe et al., 2015; Takebe et al., 2014). Undifferentiated hiPSCs were maintained on feeder-free conditions in mTeSR1 medium (StemCell technologies, Vancouver, Canada) on plates coated with Matrigel (Corning Inc., NY, USA) at 1/30 dilution at 37°C in 5% CO_2 with 95% air.

[0097] Definitive endoderm induction. Human iPSCs into definitive endoderm was differentiated using previously described methods with slight modifications (Spence et al., 2011). In brief, colonies of human iPSCs were isolated in Accutase (Thermo Fisher Scientific Inc., MA, USA) and 150,000 cells/mL were plated on Matrigel coated tissue culture plate (VWR Scientific Products, West Chester, PA). Medium was changed to RPMI 1640 medium (Life Technologies) containing 100 ng/mL Activin A (R&D Systems, MN, USA) and 50 ng/mL bone morphogenetic protein 4 (BMP4; R&D Systems) at day 1, 100 ng/mL Activin A and 0.2 % fetal calf serum (FCS; Thermo Fisher Scientific Inc.) at day 2 and 100 ng/mL Activin A and 2% FCS at day 3. Day4-6 cells were cultured in Advanced DMEM/F12 (Thermo Fisher Scientific Inc.) with B27 (Life Technologies) and N2 (Gibco, CA, USA) containing 500 ng/ml fibroblast growth factor (FGF4; R&D Systems) and 3 uM CHIR99021 (Stemgent, MA, USA). Cells were maintained at 37°C in 5% CO_2 with 95% air and the medium was replaced every day. Spheroids appeared on the plate at day 7 of differentiation.

[0098] HLO induction. At day 7, spheroids and attached cells are gently pipetted to be delaminated from dishes. They were centrifuged at 800 rpm for 3 minutes, embedded in a 100 % Matrigel drop on the dishes in Advanced DMEM/F12 with B27, N2 and 2 uM retinoic acid (RA; Sigma, MO, USA) after removing supernatant, and cultured for 4 days. After RA treatment, spheroids embedded in the Matrigel drop were cultured in Hepatocytes Culture Medium (HCM; Lonza, MD, USA) with 10 ng/mL hepatocyte growth factor (HGF; PeproTech, NJ, USA), 0.1 uM Dexamethasone (Dex; Sigma) and 20 ng/mL Oncostatin M (OSM; R&D Systems). Cultures for HLO induction were maintained at 37°C in 5% CO_2 with 95% air and the medium was

replaced every 2-3 days. To analyze HLO (day 20-30), organoids were isolated from Matrigel by scratching and pipetting.

[0099] Albumin, IL-6, and P3NP ELISA. To measure albumin secretion level of HLO, 200 μL of culture supernatant was collected from HLO embedded in Matrigel. For IL-6 and P3NP, 20-30 organoids were seeded and cultured on an ultra-low attachment multiwell plates 96 well plate (Corning). To define the exact number of organoids in each well and lastly normalize the secreted level for IL-6 and P3NP by the number, the organoids were captured on The KEYENCE BZ-X710 Fluorescence Microscope. The culture supernatants were collected at 24hrs (for albumin), 96 hrs (for IL-6) and 120 hrs (P3NP) time points after the culture and stored at -80°C until use. The supernatant was centrifuged at 1,500 rpm for 3 min and to pellet debris, and the resulting supernatant was assayed with Human Albumin ELISA Quantitation Set (Bethyl Laboratories, Inc., TX, USA), Human IL-6 ELISA Kit (Biolegend, CA, USA), and Human N-terminal procollagen III propeptide, PIIINP ELISA Kit (My BioSource, CA, USA) according to the manufacturer's instructions. Significance testing was conducted by Student's t-test.

[00100] Bile transport activity. Fluorescein diacetate was used for evaluating bile transport activity in organoids. 10 mg/mL fluorescein diacetate (Sigma) was added into HCM media cultured with HLO and allowed to sit for 5 minutes and captured using fluorescent microscopy BZ-X710 (Keyence, Osaka, Japan).

[00101] Phagocyte, lipids, ROS live-cell imaging. After being cultured in an ultra-low attachment 6 multi-well plate, 5-10 HLO were picked up and seeded in a Microslide 8 Well Glass Bottom plate (Ibidi, WI, USA) and subjected to live-cell staining. The following antibodies were used: pHrodo® Red S. aureus

Bioparticles® Conjugate for Phagocyte activity (Thermo Fisher Scientific Inc.), BODIPY® 493/503 for lipids (Thermo Fisher Scientific Inc.), Di-8-ANEPPS for membrane (Thermo Fisher Scientific Inc.), and CellROX green reagent for ROS detection (Thermo Fisher Scientific Inc.). Nuclear staining was marked by NucBlue Live ReadyProbes Reagent (Thermo Fisher Scientific Inc.). hLOHLO was visualized and scanned on a Nikon A1 Inverted Confocal Microscope (Japan) using 60× water immersion objectives. The final lipid droplet volume was calculated by IMARIS8 and normalized by each organoid size. Significance testing for lipid droplet volume and ROS production (%) was conducted by Student's t-test.

[00102] HE staining and immunohistochemistry. HLO were isolated from Matrigel and fixed in 4% paraformaldehyde and embedded in paraffin. Sections were subjected to HE and immunohistochemical staining. The following primary antibodies were used: anti-alpha smooth muscle actin antibody (1:200 dilution; abcam, Cambridge, UK), Desmin antibody (Pre-diluted; Roche, Basel, Switzerland), and CD68 antibody (1:200 dilution; abcam).

[00103] Flow cytometry. HLO were isolated from 10 Matrigel droplets and washed by 1 x PBS. HLO were dissociated to single cells by the treatment of Trypsin-EDTA (0.05%), phenol red (Gibco) for 10 min. After PBS wash, the single cells were subjected to flow cytometry with BV421-conjugated Epcam antibody (BioLegend), PE-conjugated CD166 antibody (eBioscience, CA, USA), and PE/Cy7- CD68 (eBioscience). DNA was measured by propidium iodide staining.

[00104] LPS and FFA exposure and OCA and FGF19 treatment. 20-30 HLO, which had been isolated from Matrigel and washed by 1 x

PBS, were divided into each condition and cultured on an ultra-low attachment 6 multi-well plates (Corning). HLO were cultured with LPS (Sigma), OA (Sigma), LA (Sigma), SA (Sigma), or PA (Sigma) and collected at day 1 and 3 (for LPS HLO) and at day 3 and 5 (for OA) after the culture. To test the inhibitory effect of OCA (INT-747, MedChem Express, NJ, USA) and human FGF19 recombinant (Sigma) on HLO, 20-30 HLO were cultured in HCM media in the presence or absence of oleic acid (800 μM), and 1 μM OCA and 40 ng/ ml FGF19 were added into 800μM OA condition. HLO were collected at day 3 for lipids live-cell imaging and at day 5 for stiffness measurement.

[00105] Whole mount immunofluorescence. HLO were fixed for 30 min in 4% paraformaldehyde and permeabilized for 15 min with 0.5% Nonidet P-40. HLO were washed by 1x PBS three times and incubated with blocking buffer for 1 h at room temperature. HLO were then incubated with primary antibody; anti-alpha smooth muscle actin antibody (1:50 dilution; abcam) overnight at 4 °C. HLO were washed by 1 x PBS and incubated in secondary antibody in blocking buffer for 30 min at room temperature. HLO were washed and mounted using Fluoroshield mounting medium with DAPI (abcam). The stained HLO were visualized and scanned on a Nikon A1 Inverted Confocal Microscope (Japan) using 60× water immersion objectives.

[00106] RNA isolation, RT–qPCR. RNA was isolated using the RNeasy mini kit (Qiagen, Hilden, Germany). Reverse transcription was carried out using the SuperScriptIII First-Strand Synthesis System for RT-PCR (Invitrogen, CA, USA) according to manufacturer's protocol. qPCR was carried out using TaqMan gene expression master mix (Applied Biosystems) on a QuantStudio 3 Real-Time PCR System (Thermo Fisher Scientific

Inc.). All primers and probe information for each target gene was obtained from the Universal ProbeLibrary Assay Design Center (https://qpcr.probefinder.com/organism.jsp). Significance testing was conducted by Student's t-test.

[00107] HLO stiffness measurement by AFM. HLOs treated with 0, 50200, 1400, 2800 ng/mLμM LPSOA were used for stiffness measurement with a AFM (NanoWizard IV, JPK Instruments, Germany). The AFM head with a silicon nitride cantilever (CSC37, k = 0.3 N/m, MikroMasch, Bulgaria) was mounted on a fluorescence stereo microscope (M205 FA, Leica, Germany) coupled with a Z-axis piezo stage (JPK CellHesion module, JPK Instruments, Germany), which allows the indentation measurement up to the depth of ~ 100 μm. As a substrate for organoids, a fibronectin-coated dish was used. The tissue culture dish (φ = 34 mm, TPP Techno Plastic Products, Switzerland) was first incubated with a 1 μg/mL fibronectin solution (Sigma)) at 4 °C for overnight. Then, the tissue culture dish was washed twice by distilled water and dried for 1 hour. Thereafter, HLOs incubated with OALPS for 51 days were deposited to the fibronectin-coated dish and incubated for 1 hour at 37°C. The sample dish was then placed onto the AFM stage, and force-distance curves in a 14 × 14 matrix in a 25 × 25 μm square were measured from each HLO. Finally, Young's moduli (E, Pa) of HLO were determined by fitting the obtained force-distance curves with the modified Hertz model (Sneddon, 1965). Dunn-Holland-Wolfe test was performed for significance testings.

[00108] THP-1 cell migration assay. THP-1 cell, which was gifted from T. Suzuki, was maintained in Advanced DMEM/F12 (Thermo Fisher Scientific Inc.) containing 10% FBS. THP-1 floating cells were collected, and 200,000 cells were added with serum-free

Advanced DMEM/F12 to the membrane chamber of the CytoSelect™ 96-Well Cell Migration Assay (5 μm, Fluorometric Format; Cell Biolabs, CA, USA). 10-20 HLO were cultured in HCM media including 0, 400, 800uM OA with an ultra-low attachment 96 multi-well plate (Corning) for three days. To define the exact number of organoids in each well and lastly normalize the final migrated cells by the number, the organoids were captured on The KEYENCE BZ-X710 Fluorescence Microscope. 150 μL of culture supernatant of HLO was collected and added to the feeder tray of the kit. The kit was incubated at 37°C for 24 h in a 5% CO_2 cell culture incubator. Cells that had migrated were counted using Countess II FL Automated Cell Counter (Thermo Fisher Scientific Inc.). Significance testing was conducted by Student's t-test.

[00109] Triglyceride assay. For quantitative determination of triglycerides, HLO were isolated from one Matrigel drop and divided into HCM media in the presence or absence of oleic acid (800 μM). They were cultured on an ultra-Low attachment 6 multi-well plate for three days. Quantitative estimation of hepatic triglyceride accumulation was performed by an enzymatic assay of triglyceride mass using the EnzyChrom Triglyceride assay kit (Bioassay Systems, CA, USA).

[00110] HLO survival assay. HLO were collected from Matrigel and washed by 1 x PBS. 30-40 organoids were cultured on an ultra-low attachment 6 multi-well plate (Corning). HLO were captured on The KEYENCE BZ-X710 Fluorescence Microscope every day. The surviving and dead organoids were counted manually from the photo. HLO with a rounded configuration was counted as the surviving while the organoids with out of shape is counted as dead. To assess the survival rate of OA treated HLO at the

same time point, 3D cell titer glo assay was used (Promega, Wi, USA).

[00111] Statistics and reproducibility. Statistical analysis was performed using unpaired two- tailed Student's t-test, Dunn-Holland-Wolfe test, or Welch's t-test. Results were shown mean ± s.e.m.; P values < 0.05 were considered statistically significant. N-value refers to biologically independent replicates, unless noted otherwise.

[00112] References

[00113] Ajmera, V., Perito, E.R., Bass, N.M., Terrault, N.A., Yates, K.P., Gill, R., Loomba, R., Diehl, A.M., Aouizerat, B.E., and Network, N.C.R. (2017). Novel plasma biomarkers associated with liver disease severity in adults with nonalcoholic fatty liver disease. Hepatology 65, 65-77.

[00114] Bahar Halpern, K., Shenhav, R., Matcovitch-Natan, O., Toth, B., Lemze, D., Golan, M., Massasa, E.E., Baydatch, S., Landen, S., Moor, A.E., et al. (2017). Single-cell spatial reconstruction reveals global division of labour in the mammalian liver. Nature 542, 352-356.

[00115] Boullata, J.I., Gilbert, K., Sacks, G., Labossiere, R.J., Crill, C., Goday, P., Kumpf, V.J., Mattox, T.W., Plogsted, S., Holcombe, B., et al. (2014). A.S.P.E.N. clinical guidelines: parenteral nutrition ordering, order review, compounding, labeling, and dispensing. JPEN J Parenter Enteral Nutr 38, 334-377.

[00116] Chen, Y., Pan, F.C., Brandes, N., Afelik, S., Solter, M., and Pieler, T. (2004). Retinoic acid signaling is essential for pancreas development and promotes endocrine at the expense of exocrine cell differentiation in Xenopus. Dev Biol 271, 144-160.

[00117] Dash, A., Figler, R.A., Blackman, B.R., Marukian, S., Collado, M.S., Lawson, M.J., Hoang, S.A., Mackey, A.J., Manka, D., Cole, B.K., et al. (2017). Pharmacotoxicology of clinically-relevant concentrations of obeticholic acid in an organotypic human hepatocyte system. Toxicol In Vitro 39, 93-103.

[00118] El Kasmi, K.C., Anderson, A.L., Devereaux, M.W., Vue, P.M., Zhang, W., Setchell, K.D., Karpen, S.J., and Sokol, R.J. (2013). Phytosterols promote liver injury and Kupffer cell activation in parenteral nutrition-associated liver disease. Sci Transl Med 5, 206ra137.

[00119] El Taghdouini, A., Najimi, M., Sancho-Bru, P., Sokal, E., and van Grunsven, L.A. (2015). In vitro reversion of activated primary human hepatic stellate cells. Fibrogenesis Tissue Repair 8, 14.

[00120] Geerts, A., Eliasson, C., Niki, T., Wielant, A., Vaeyens, F., and Pekny, M. (2001). Formation of normal desmin intermediate filaments in mouse hepatic stellate cells requires vimentin. Hepatology 33, 177-188.

[00121] Hassan, W., Rongyin, G., Daoud, A., Ding, L., Wang, L., Liu, J., and Shang, J. (2014). Reduced oxidative stress contributes to the lipid lowering effects of isoquercitrin in free fatty acids induced hepatocytes. Oxid Med Cell Longev 2014, 313602.

[00122] Hynds, R.E., and Giangreco, A. (2013). Concise review: the relevance of human stem cell-derived organoid models for epithelial translational medicine. Stem Cells 31, 417-422.

[00123] Ijpenberg, A., Perez-Pomares, J.M., Guadix, J.A., Carmona, R., Portillo-Sanchez, V., Macias, D., Hohenstein, P., Miles, C.M., Hastie, N.D., and Munoz-Chapuli, R. (2007). Wt1 and retinoic

acid signaling are essential for stellate cell development and liver morphogenesis. Dev Biol 312, 157-170.

[00124] Ito, K., Sakuma, S., Kimura, M., Takebe, T., Kaneko, M., and Arai, F. (2016). Temporal Transition of Mechanical Characteristics of HUVEC/MSC Spheroids Using a Microfluidic Chip with Force Sensor Probes. Micromachines-Basel 7.

[00125] Kanuri, G., and Bergheim, I. (2013). In vitro and in vivo models of non-alcoholic fatty liver disease (NAFLD). Int J Mol Sci 14, 11963-11980.

[00126] Kelly, G.M., and Drysdale, T.A. (2015). Retinoic Acid and the Development of the Endoderm. J Dev Biol 3, 25-56.

[00127] Koehler, E.M., Plompen, E.P., Schouten, J.N., Hansen, B.E., Darwish Murad, S., Taimr, P., Leebeek, F.W., Hofman, A., Stricker, B.H., Castera, L., et al. (2016). Presence of diabetes mellitus and steatosis is associated with liver stiffness in a general population: The Rotterdam study. Hepatology 63, 138-147.

[00128] Kordes, C., Sawitza, I., Gotze, S., Herebian, D., and Haussinger, D. (2014). Hepatic stellate cells contribute to progenitor cells and liver regeneration. J Clin Invest 124, 5503-5515.

[00129] Kumar, J.A., and Teckman, J.H. (2015). Controversies in the Mechanism of Total Parenteral Nutrition Induced Pathology. Children (Basel) 2, 358-370.

[00130] Lancaster, M.A., and Knoblich, J.A. (2014). Organogenesis in a dish: modeling development and disease using organoid technologies. Science 345, 1247125.

[00131] McCracken, K.W., Aihara, E., Martin, B., Crawford, C.M., Broda, T., Treguier, J., Zhang, X., Shannon, J.M., Montrose,

M.H., and Wells, J.M. (2017). Wnt/beta-catenin promotes gastric fundus specification in mice and humans. Nature 541, 182-187.

[00132] Mercaldi, C.J., Reynolds, M.W., and Turpin, R.S. (2012). Methods to identify and compare parenteral nutrition administered from hospital-compounded and premixed multichamber bags in a retrospective hospital claims database. JPEN J Parenter Enteral Nutr 36, 330-336.

[00133] Nandivada, P., Carlson, S.J., Chang, M.I., Cowan, E., Gura, K.M., and Puder, M. (2013). Treatment of parenteral nutrition-associated liver disease: the role of lipid emulsions. Adv Nutr 4, 711-717.

[00134] Negishi, T., Nagai, Y., Asaoka, Y., Ohno, M., Namae, M., Mitani, H., Sasaki, T., Shimizu, N., Terai, S., Sakaida, I., et al. (2010). Retinoic acid signaling positively regulates liver specification by inducing wnt2bb gene expression in medaka. Hepatology 51, 1037-1045.

[00135] Neuschwander-Tetri, B.A., Loomba, R., Sanyal, A.J., Lavine, J.E., Van Natta, M.L., Abdelmalek, M.F., Chalasani, N., Dasarathy, S., Diehl, A.M., Hameed, B., et al. (2015). Farnesoid X nuclear receptor ligand obeticholic acid for non-cirrhotic, non-alcoholic steatohepatitis (FLINT): a multicentre, randomised, placebo-controlled trial. Lancet 385, 956-965.

[00136] Orso, G., Mandato, C., Veropalumbo, C., Cecchi, N., Garzi, A., and Vajro, P. (2016). Pediatric parenteral nutrition-associated liver disease and cholestasis: Novel advances in pathomechanisms-based prevention and treatment. Dig Liver Dis 48, 215-222.

[00137] Purton, L.E., Bernstein, I.D., and Collins, S.J. (2000). All-trans retinoic acid enhances the long-term repopulating activity of cultured hematopoietic stem cells. Blood 95, 470-477.

[00138] Ronn, R.E., Guibentif, C., Moraghebi, R., Chaves, P., Saxena, S., Garcia, B., and Woods, N.B. (2015). Retinoic acid regulates hematopoietic development from human pluripotent stem cells. Stem Cell Reports 4, 269-281.

[00139] Saini, A. (2016). Cystic Fibrosis Patients Benefit from Mini Guts. Cell Stem Cell 19, 425-427.

[00140] Spence, J.R., Mayhew, C.N., Rankin, S.A., Kuhar, M.F., Vallance, J.E., Tolle, K., Hoskins, E.E., Kalinichenko, V.V., Wells, S.I., Zorn, A.M., et al. (2011). Directed differentiation of human pluripotent stem cells into intestinal tissue in vitro. Nature 470, 105-109.

[00141] Stafford, D., Hornbruch, A., Mueller, P.R., and Prince, V.E. (2004). A conserved role for retinoid signaling in vertebrate pancreas development. Dev Genes Evol 214, 432-441.

[00142] Stender, S., Kozlitina, J., Nordestgaard, B.G., Tybjaerg-Hansen, A., Hobbs, H.H., and Cohen, J.C. (2017). Adiposity amplifies the genetic risk of fatty liver disease conferred by multiple loci. Nat Genet 49, 842-847.

[00143] Takebe, T., Enomura, M., Yoshizawa, E., Kimura, M., Koike, H., Ueno, Y., Matsuzaki, T., Yamazaki, T., Toyohara, T., Osafune, K., et al. (2015). Vascularized and Complex Organ Buds from Diverse Tissues via Mesenchymal Cell-Driven Condensation. Cell Stem Cell 16, 556-565.

[00144] Takebe, T., Sekine, K., Enomura, M., Koike, H., Kimura, M., Ogaeri, T., Zhang, R.R., Ueno, Y., Zheng, Y.W., Koike, N., et al.

(2013). Vascularized and functional human liver from an iPSC-derived organ bud transplant. Nature 499, 481-484.

[00145] Takebe, T., Zhang, R.R., Koike, H., Kimura, M., Yoshizawa, E., Enomura, M., Koike, N., Sekine, K., and Taniguchi, H. (2014). Generation of a vascularized and functional human liver from an iPSC-derived organ bud transplant. Nat Protoc 9, 396-409.

[00146] Tsedensodnom, O., and Sadler, K.C. (2013). ROS: redux and paradox in fatty liver disease. Hepatology 58, 1210-1212.

[00147] van de Garde, M.D., Movita, D., van der Heide, M., Herschke, F., De Jonghe, S., Gama, L., Boonstra, A., and Vanwolleghem, T. (2016). Liver Monocytes and Kupffer Cells Remain Transcriptionally Distinct during Chronic Viral Infection. PLoS One 11, e0166094.

[00148] Wang, Y., Li, J., Wang, X., Sang, M., and Ho, W. (2013). Hepatic stellate cells, liver innate immunity, and hepatitis C virus. J Gastroenterol Hepatol 28 Suppl 1, 112-115.

[00149] Warren, C.R., Jaquish, C.E., and Cowan, C.A. (2017a). The NextGen Genetic Association Studies Consortium: A Foray into In Vitro Population Genetics. Cell Stem Cell 20, 431-433.

[00150] Warren, C.R., O'Sullivan, J.F., Friesen, M., Becker, C.E., Zhang, X., Liu, P., Wakabayashi, Y., Morningstar, J.E., Shi, X., Choi, J., et al. (2017b). Induced Pluripotent Stem Cell Differentiation Enables Functional Validation of GWAS Variants in Metabolic Disease. Cell Stem Cell 20, 547-557 e547.

[00151] Workman, M.J., Mahe, M.M., Trisno, S., Poling, H.M., Watson, C.L., Sundaram, N., Chang, C.F., Schiesser, J., Aubert, P., Stanley, E.G., et al. (2017). Engineered human pluripotent-stem-

cell-derived intestinal tissues with a functional enteric nervous system. Nat Med 23, 49-59.

[00152] Xu, R., Tao, A., Zhang, S., Deng, Y., and Chen, G. (2015). Association between patatin-like phospholipase domain containing 3 gene (PNPLA3) polymorphisms and nonalcoholic fatty liver disease: a HuGE review and meta-analysis. Sci Rep 5, 9284.

[00153] Yanagimachi, M.D., Niwa, A., Tanaka, T., Honda-Ozaki, F., Nishimoto, S., Murata, Y., Yasumi, T., Ito, J., Tomida, S., Oshima, K., et al. (2013). Robust and highly-efficient differentiation of functional monocytic cells from human pluripotent stem cells under serum- and feeder cell-free conditions. PLoS One 8, e59243.

[00154] Yoneda, M., Yoneda, M., Mawatari, H., Fujita, K., Endo, H., Iida, H., Nozaki, Y., Yonemitsu, K., Higurashi, T., Takahashi, H., et al. (2008). Noninvasive assessment of liver fibrosis by measurement of stiffness in patients with nonalcoholic fatty liver disease (NAFLD). Dig Liver Dis 40, 371-378.

[00155] Zain, S.M., Mohamed, Z., and Mohamed, R. (2015). Common variant in the glucokinase regulatory gene rs780094 and risk of nonalcoholic fatty liver disease: a meta-analysis. J Gastroenterol Hepatol 30, 21-27.

[00156] Zambrano, E., El-Hennawy, M., Ehrenkranz, R.A., Zelterman, D., and Reyes-Mugica, M. (2004). Total parenteral nutrition induced liver pathology: an autopsy series of 24 newborn cases. Pediatr Dev Pathol 7, 425-432.

[00157] Zorn, A.M., and Wells, J.M. (2009). Vertebrate endoderm development and organ formation. Annu Rev Cell Dev Biol 25, 221-251.

CLAIMS

What is claimed is:

1. A method of making a lipotoxic organoid model, comprising the steps of contacting a liver organoid with a free fatty acid (FFA) composition, wherein said FFA composition comprises oleic acid, linoleic acid, palmitic acid, or combinations thereof, preferably oleic acid.

2. The method of claim 1, wherein said lipotoxic organoid model is a model of fatty liver disease.

3. The method of claim 1, wherein said lipotoxic organoid model is a model of steatohepatitis.

4. The method of claim 1, wherein said lipotoxic organoid model is a model of cirrhosis.

5. The method of claim 1, wherein said lipotoxic organoid model is a model of parenteral nutrition associated liver disease (PNALD).

6. The method of claim 1, wherein said lipotoxic organoid model is a model of NAFLD.

7. The method of any preceding claim, wherein said lipotoxic organoid model is characterized by cytoskeleton filament disorganization, ROS increase, mitochondrial swelling, trigycleride accumulation, fibrosis, hepatocyte ballooning, IL6 secretion, steatosis, inflammation, ballooning and Mallory's body-like, tissue stiffening, cell-death, and combinations thereof.

8. A method of screening for a drug for treatment of a liver disease, including NAFLD and/or cholestasis, comprising the step of contacting a candidate drug with the lipotoxic organoid model of claim 1.

9. A method of assaying the effectiveness of a nutritional supplement/TPN, comprising the step of contacting said nutritional supplement/TPN with the lipotoxic organoid model of claim 1.

10. A three-dimensional (3D) liver organoid model of fatty liver disease, wherein said organoid is characterized by steatosis, inflammation, ballooning and Mallory's bodies, ROS accumulation and mitochondrial overload; fibrosis and tissue stiffening, and cell death.

11. A three-dimensional (3D) liver organoid model of drug induced hepatotoxicity and inflammation/fibrosis.

12. A three-dimensional (3D) liver organoid model of parenteral nutrition associated liver disease (PNALD)

13. The liver organoid model according to any preceding claim, wherein said model does not comprise inflammatory cells, for example T-cells or other inflammatory secreted proteins.

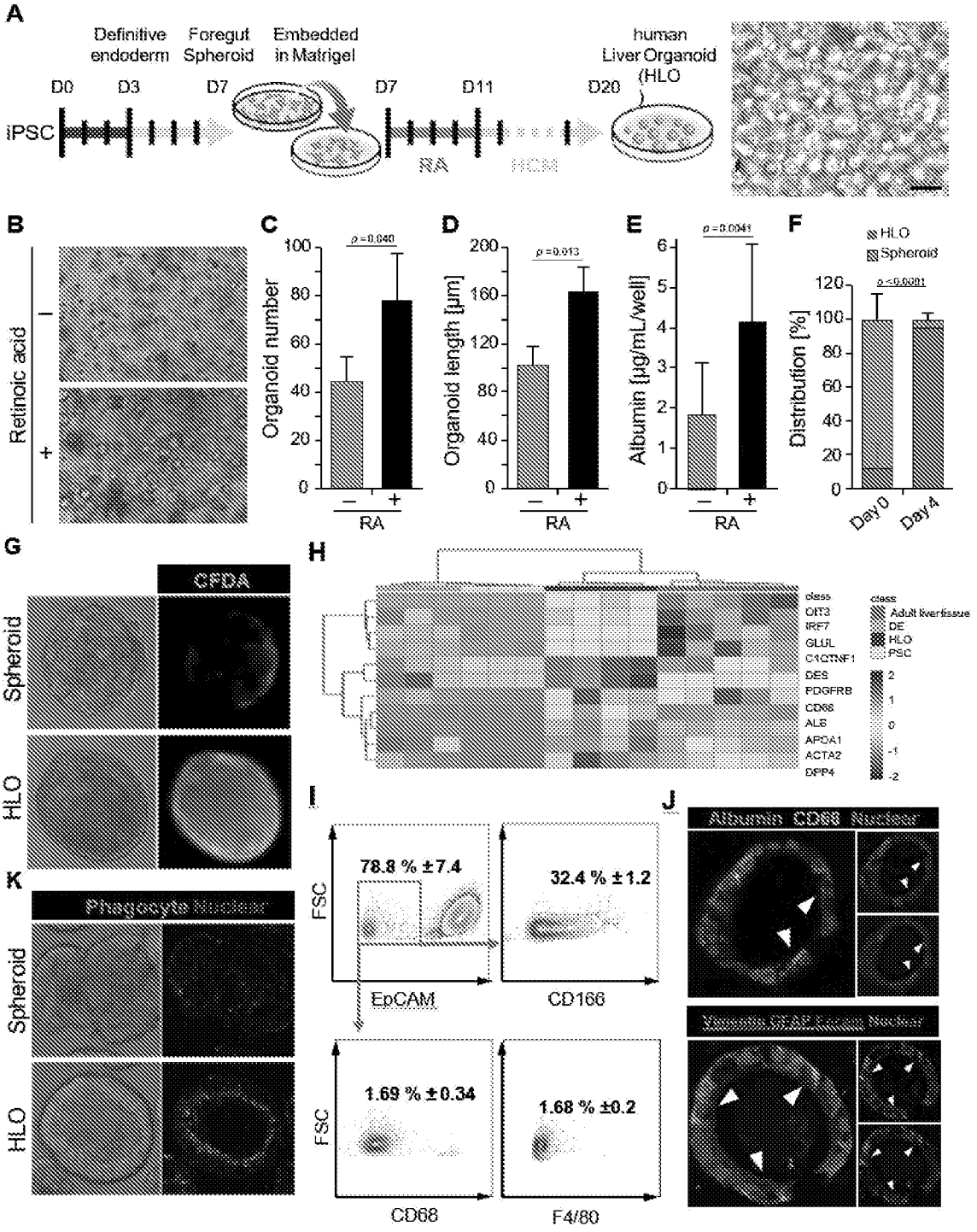
A
Definitive endoderm
Foregut Spheroid
Embedded in Matrigel
human Liver Organoid (HLO)
D0
D3
D7
D7
D11
D20
iPSC
RA
HCM
B
Retinoic acid
C
Organoid number
p = 0.040
D
Organoid length [µm]
p = 0.013
E
Albumin [µg/mL/well]
p = 0.0041
F
HLO
Spheroid
Distribution [%]
p < 0.0001
Day0
Day4
RA
G
CFDA
Spheroid
HLO
H
class
OIT3
IRF7
GLUL
C1QTNF1
DES
PDGFRB
CD68
ALB
APOA1
ACTA2
DPP4
Adult liver tissue
DE
HLO
PSC
I
78.8 % ±7.4
32.4 % ±1.2
FSC
EpCAM
CD166
1.69 % ±0.34
1.68 % ±0.2
CD68
F4/80
J
Albumin CD68 Nuclei
Vimentin CK18 Laminin Nuclei
K
Phagocyte Nuclei
Spheroid
HLO

FIG. 1

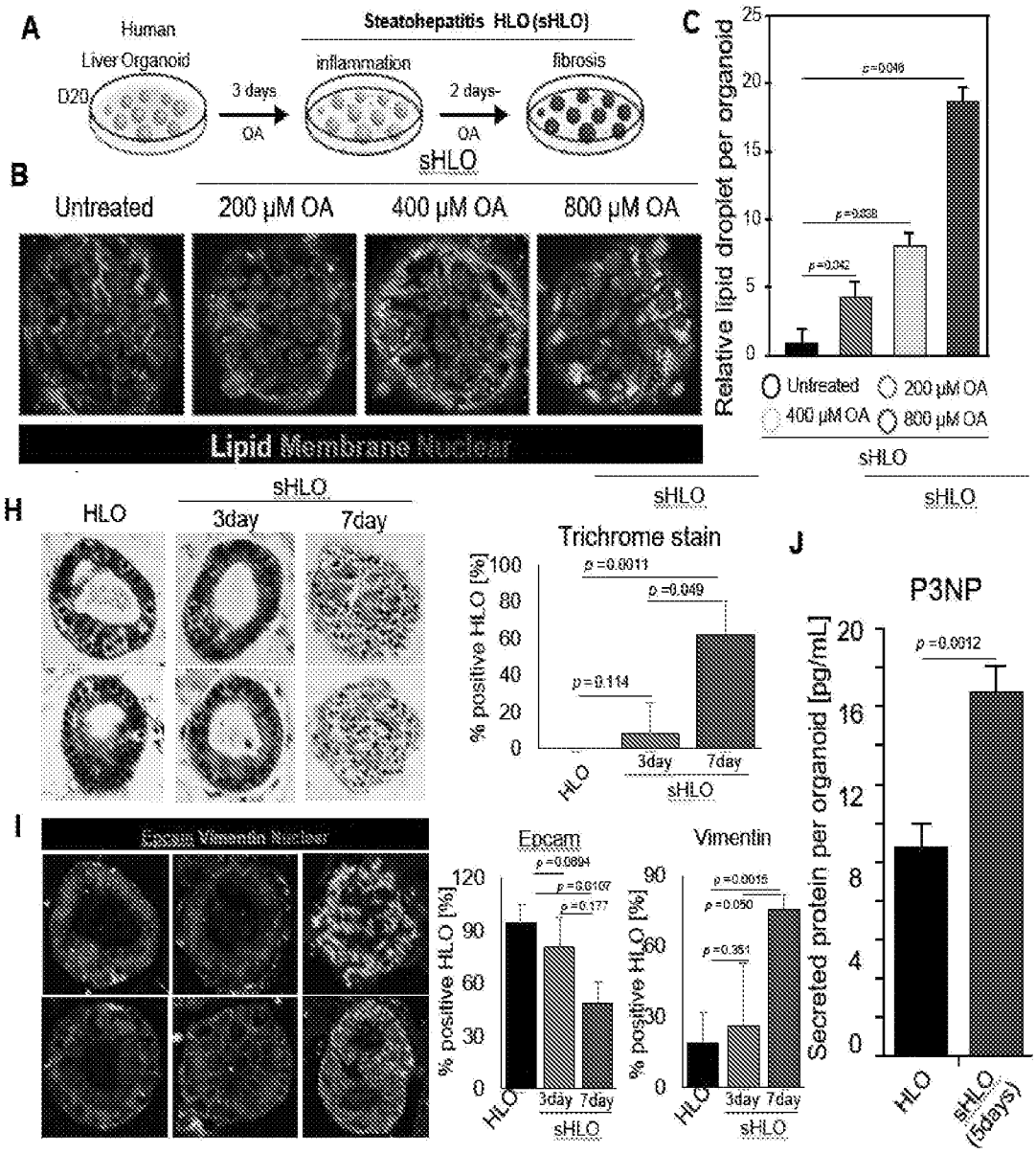
A
Human
Liver Organoid
D20
3 days
OA
Steatohepatitis HLO (sHLO)
inflammation
2 days-
OA
fibrosis
sHLO
B
Untreated
200 μM OA
400 μM OA
800 μM OA
Lipid Membrane Nuclear
C
Relative lipid droplet per organoid
p=0.046
p=0.038
p=0.042
Untreated
200 μM OA
400 μM OA
800 μM OA
sHLO
H
HLO
sHLO
3day
7day
Trichrome stain
% positive HLO [%]
p=0.0011
p=0.049
p=0.114
HLO
3day
7day
sHLO
J
P3NP
Secreted protein per organoid [pg/mL]
p=0.0012
HLO
sHLO (5days)
I
Epcam
Vimentin
% positive HLO [%]
p=0.0894
p=0.0107
p=0.177
p=0.0015
p=0.050
p=0.351
HLO
3day
7day
sHLO

FIG. 2

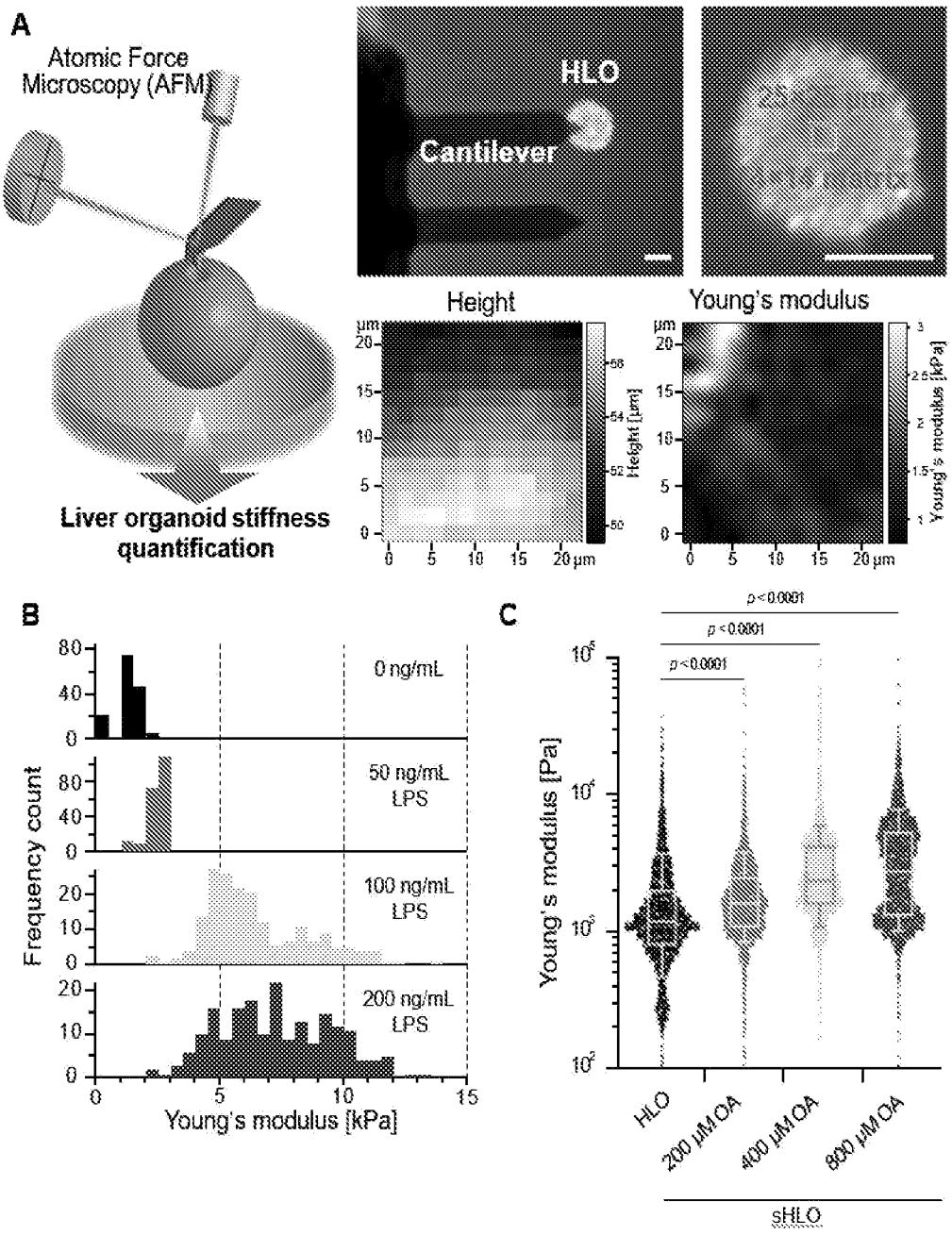
A
Atomic Force Microscopy (AFM)
Liver organoid stiffness quantification
HLO
Cantilever
Height
Young's modulus
B
Frequency count
0 ng/mL
50 ng/mL LPS
100 ng/mL LPS
200 ng/mL LPS
Young's modulus [kPa]
C
Young's modulus [Pa]
p<0.0001
HLO
200 μM OA
400 μM OA
800 μM OA
sHLO

FIG. 3

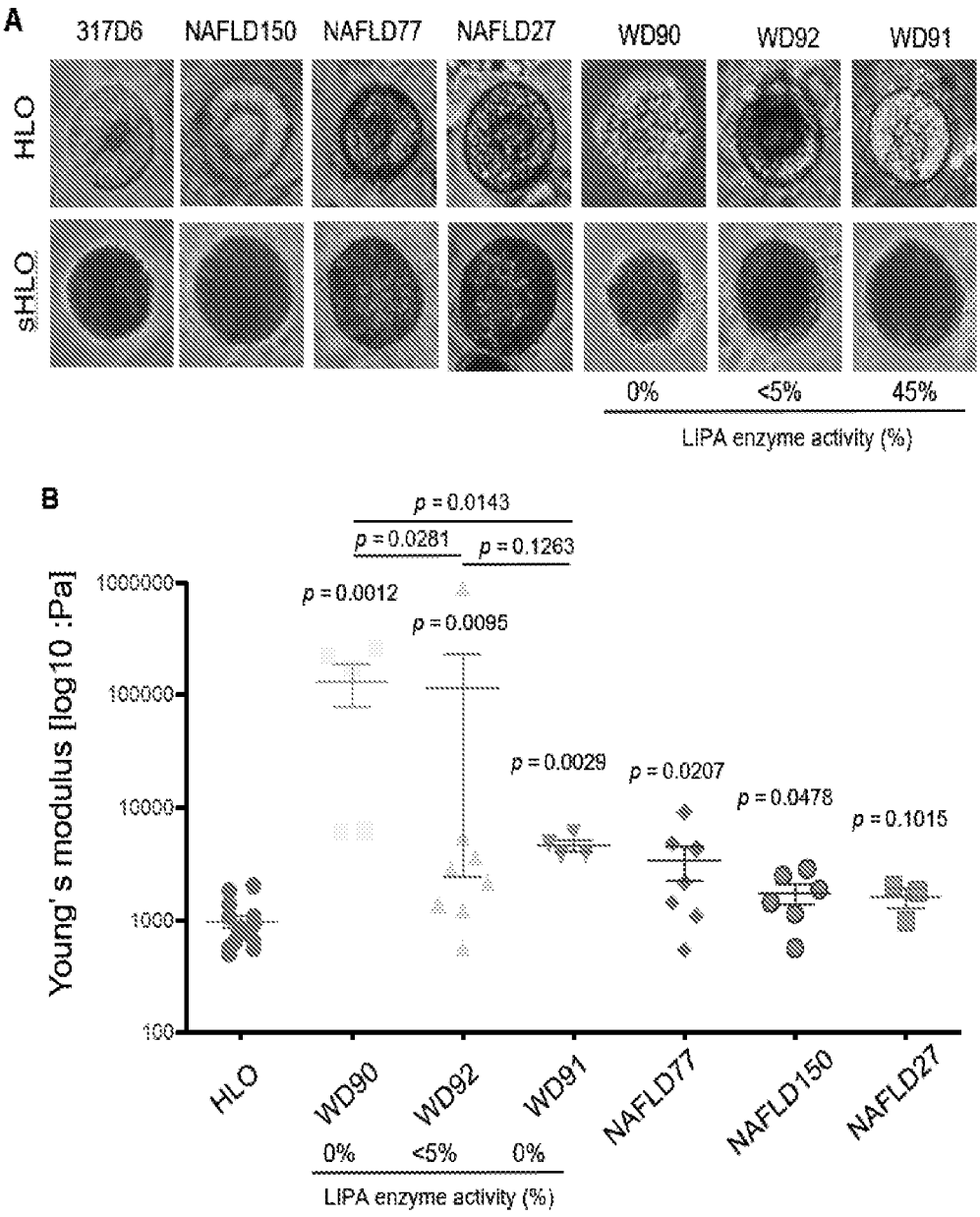
A
317D6
NAFLD150
NAFLD77
NAFLD27
WD90
WD92
WD91
HLO
sHLO
0%
<5%
45%
LIPA enzyme activity (%)
B
p = 0.0143
p = 0.0281
p = 0.1263
p = 0.0012
p = 0.0095
p = 0.0029
p = 0.0207
p = 0.0478
p = 0.1015
Young's modulus [log10 :Pa]
1000000
100000
10000
1000
100
HLO
WD90
WD92
WD91
NAFLD77
NAFLD150
NAFLD27
0%
<5%
0%
LIPA enzyme activity (%)

FIG. 4

FIG. 5A

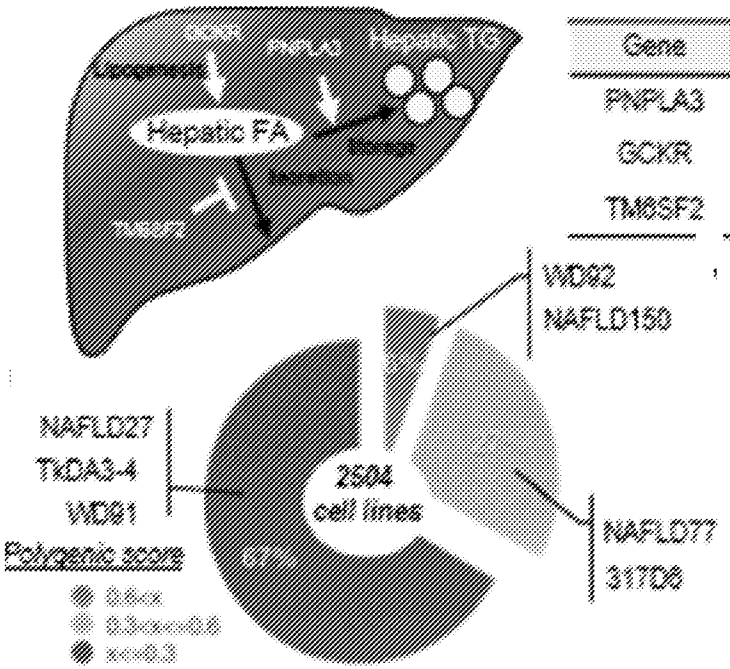

FIG. 5B

Gene	SNP	Mode of action	Hepatic TG	Circulating Lipids
PNPLA3	rs738409	lipid droplets	↑	=
GCKR	rs1260360	hepatic lipogenesis	↑	↑
TM6SF2	rs58542926	lipoprotein secretion	↑	↓

Protein	PNPLA3 p.I148M	GCKR p.P446L	TM6SF2 p.E167K	Polygenic Risk Score of 3 SNPs	Population	Ancestral Population
rs ID	rs738409	rs1260326	rs58542926			
beta for HTG0	0.26	0.08	0.29			
Donor name	G	T	T			
VID82	1	2	1	0.71	TSI,CEU	EUR
NAFLD150	2	2	0	0.60	MXL	AMR
NAFLD77	1	1	0	0.34	MXL	AMR
317D8	1	1	0	0.34	CEU	EUR
NAFLD27	1	0	0	0.26	TSI	EUR
VID91	0	2	0	0.18	CEU	EUR
TKDa	0	1	0	0.08	TSI	EUR
VID90	0	1	0	0.08	CEU	EUR

FIG. 5C

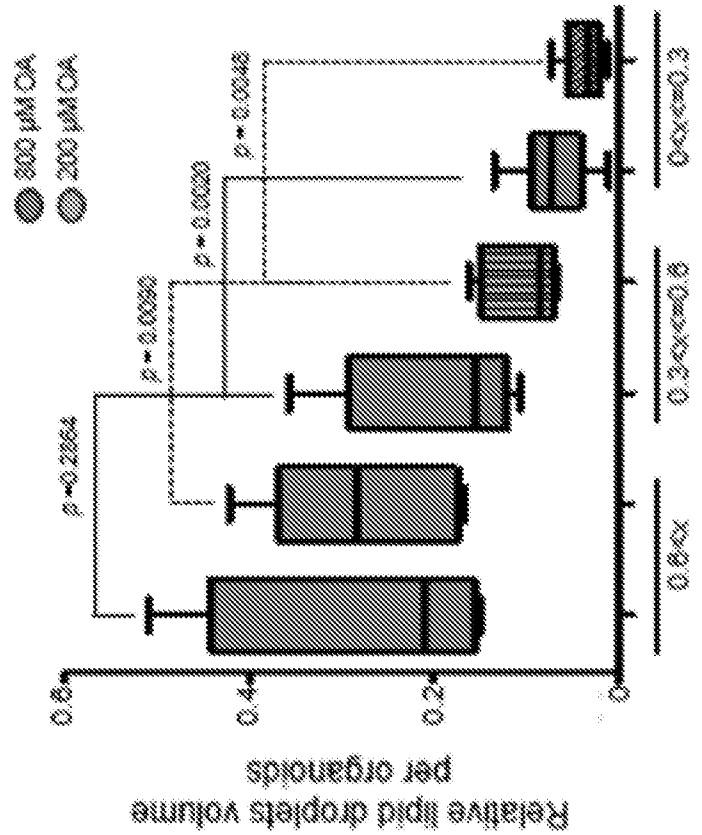
800 μM OA
200 μM OA
p = 0.2264
p = 0.0030
p = 0.0020
p = 0.0048
0.6<x
0.3<x<=0.6
0<x<=0.3
0.6
0.4
0.2
0
Relative lipid droplets volume
per organoids

FIG. 5E

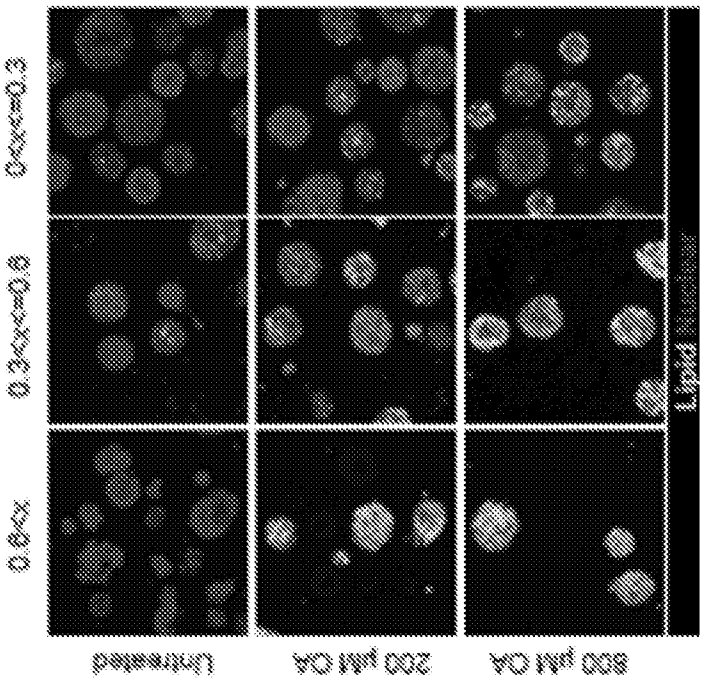
Untreated
200 μM OA
800 μM OA
0.6<x
0.3<x<=0.6
0<x<=0.3
Lipid

FIG. 5D

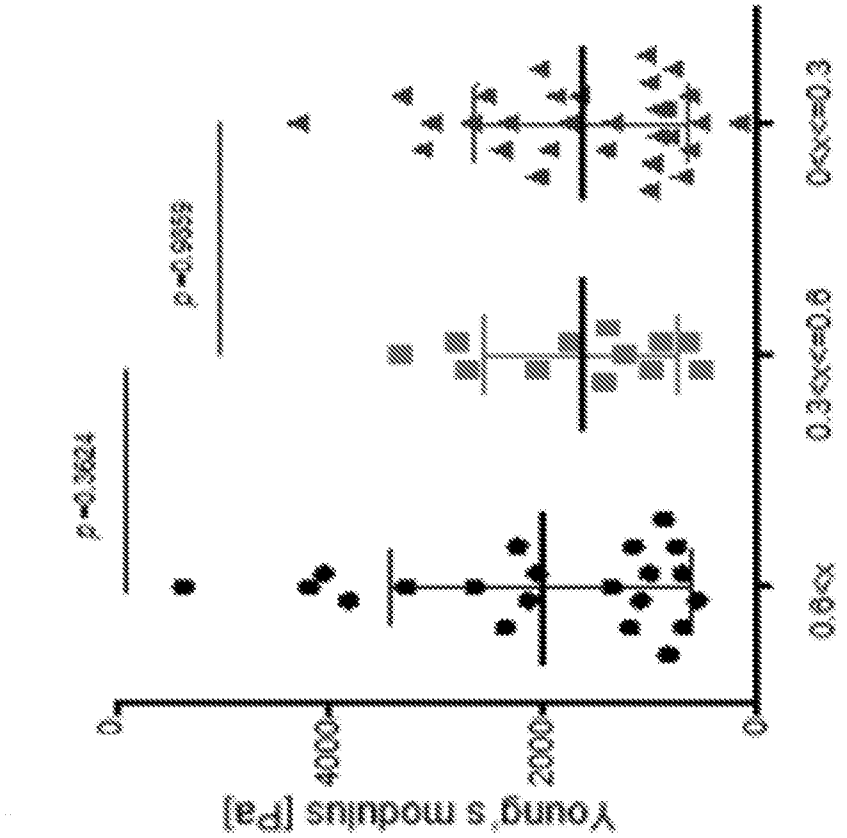
Young's modulus [Pa]
p=0.3924
p=0.0009
0.6<x
0.3<x<=0.6
0<x<=0.3

FIG. 5G

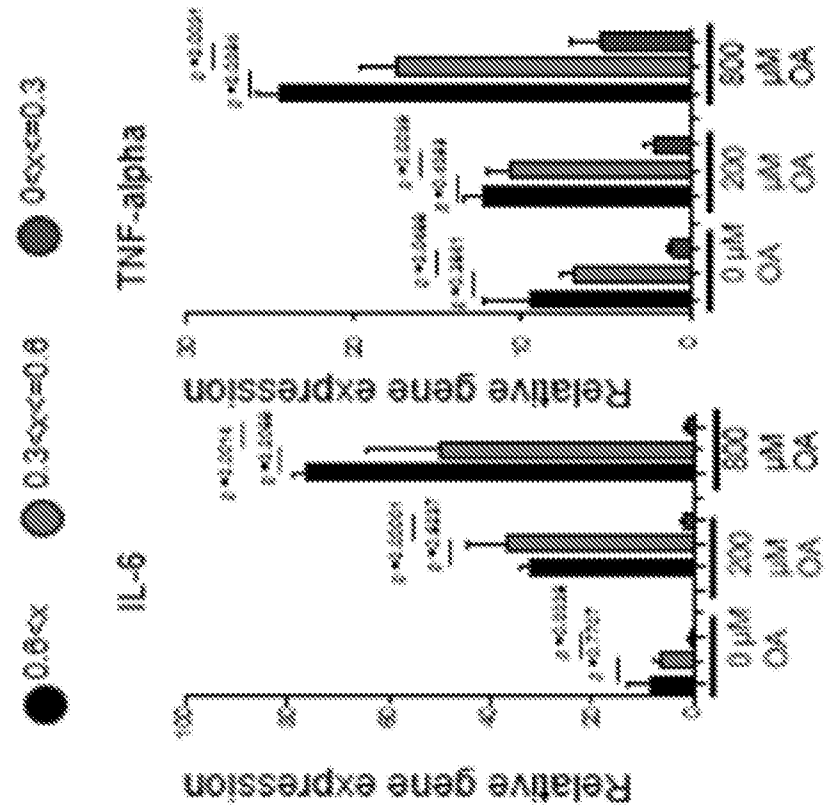
0.6<x
0.3<x<=0.6
0<x<=0.3
IL-6
TNF-alpha
Relative gene expression
0 μM OA
200 μM OA
600 μM OA

FIG. 5F

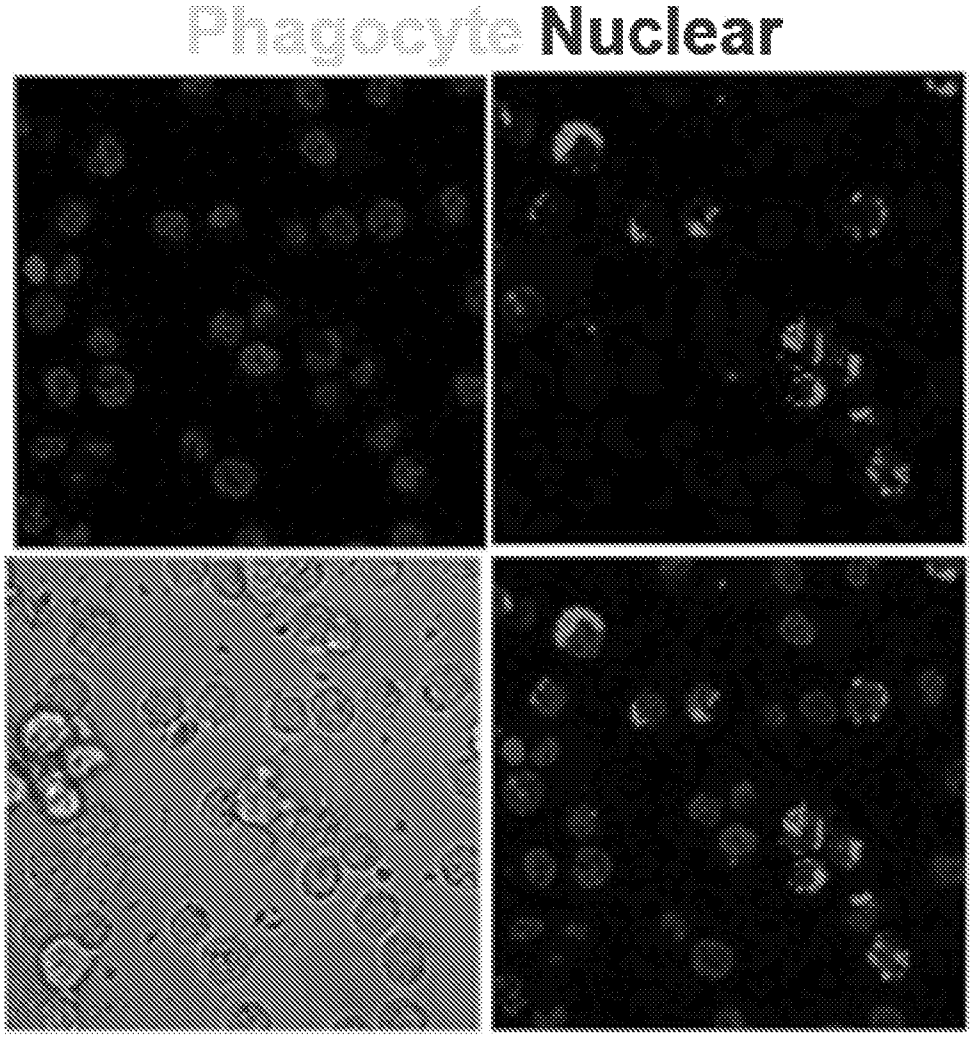

FIG. 6

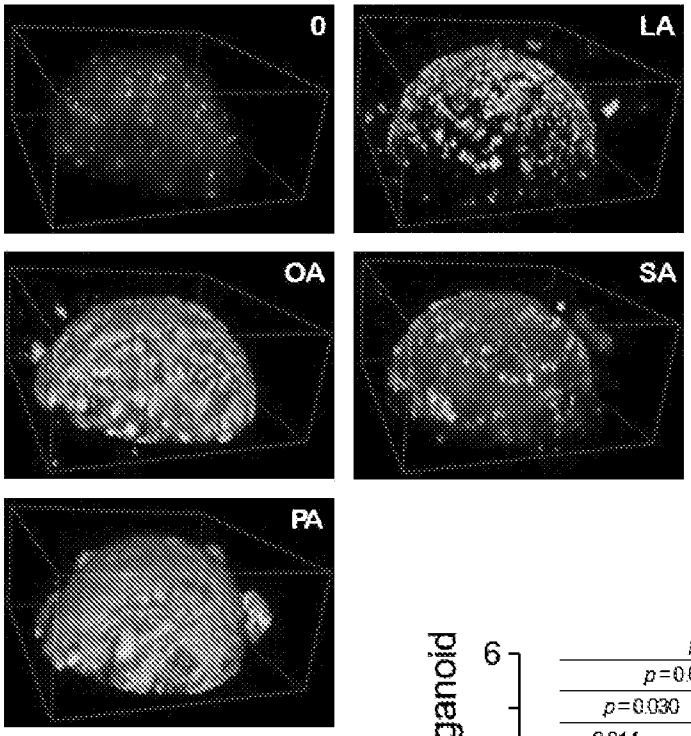
0
LA
OA
SA
PA

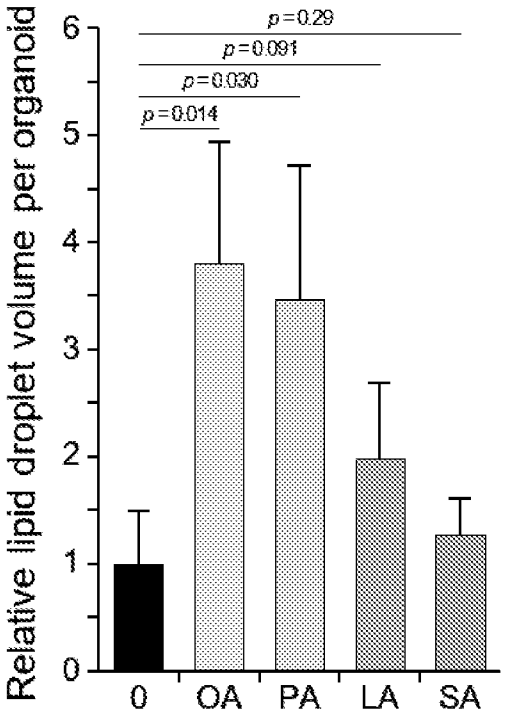
p=0.29
p=0.091
p=0.030
p=0.014
Relative lipid droplet volume per organoid
0
1
2
3
4
5
6
0
OA
PA
LA
SA

FIG. 7

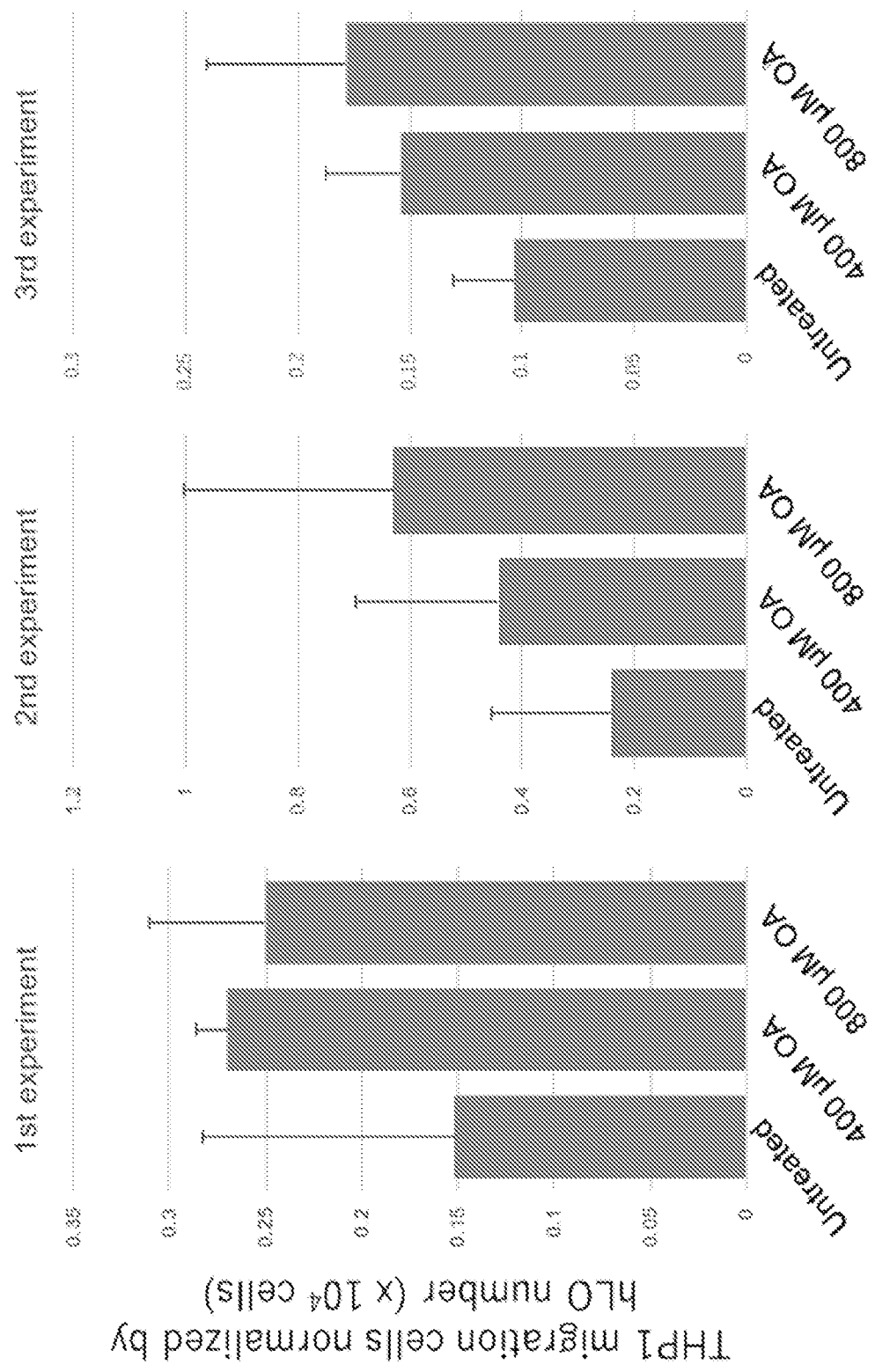
THP1 migration cells normalized by
hLO number (x 10⁴ cells)
1st experiment
2nd experiment
3rd experiment
Untreated
400 μM OA
800 μM OA
0
0.05
0.1
0.15
0.2
0.25
0.3
0.35
0.4
0.6
0.8
1
1.2

FIG. 8

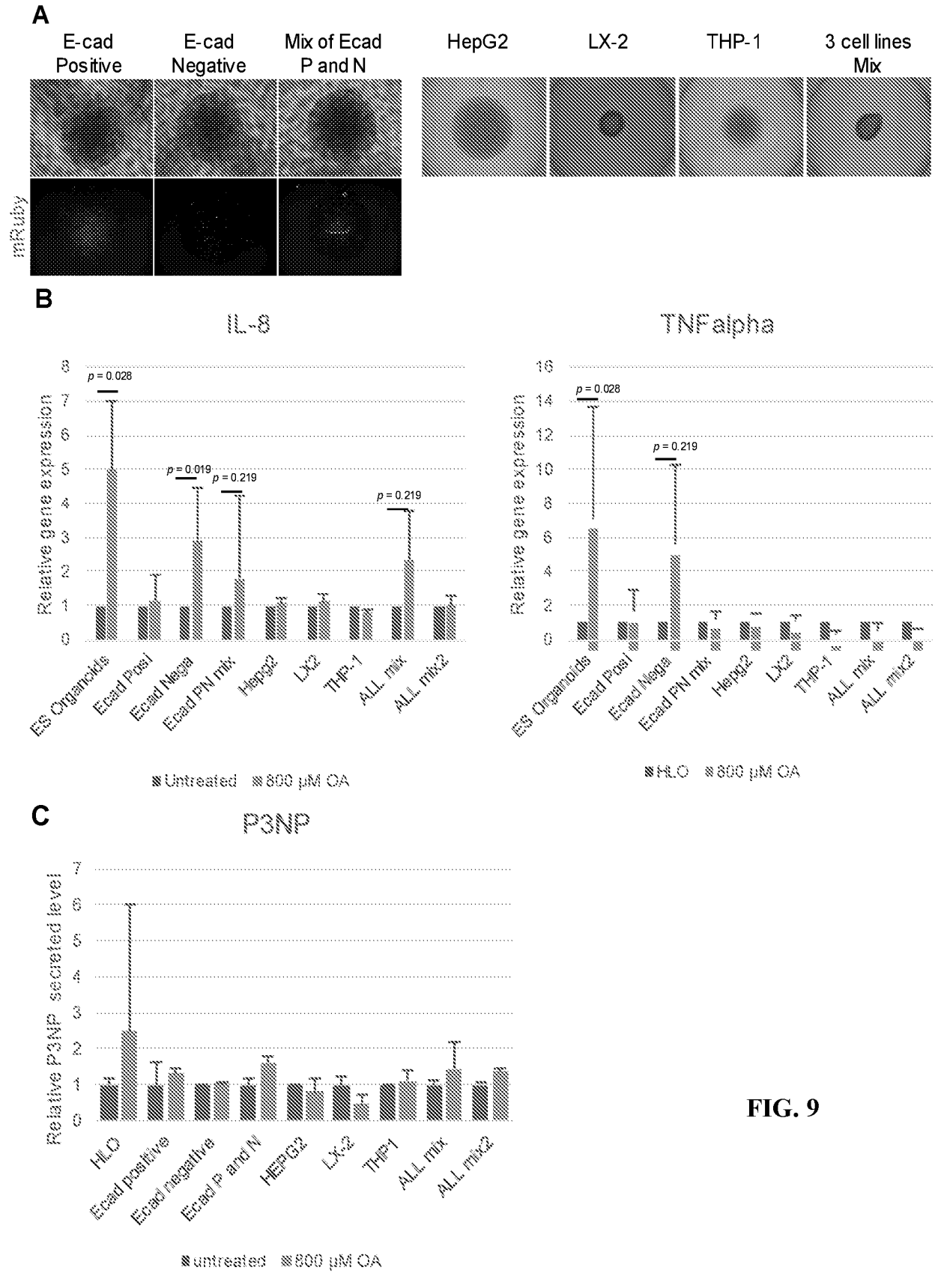
A
E-cad Positive
E-cad Negative
Mix of Ecad P and N
HepG2
LX-2
THP-1
3 cell lines Mix
mRuby
B
IL-8
Relative gene expression
p = 0.028
p = 0.019
p = 0.219
p = 0.219
ES Organoids
Ecad Posi
Ecad Nega
Ecad PN mix
Hepg2
LX2
THP-1
ALL mix
ALL mix2
Untreated
800 μM OA
TNFalpha
Relative gene expression
p = 0.028
p = 0.219
ES Organoids
Ecad Posi
Ecad Nega
Ecad PN mix
Hepg2
LX2
THP-1
ALL mix
ALL mix2
HLO
800 μM OA
C
P3NP
Relative P3NP secreted level
HLO
Ecad positive
Ecad negative
Ecad P and N
HEPG2
LX-2
THP1
ALL mix
ALL mix2
untreated
800 μM OA

FIG. 9

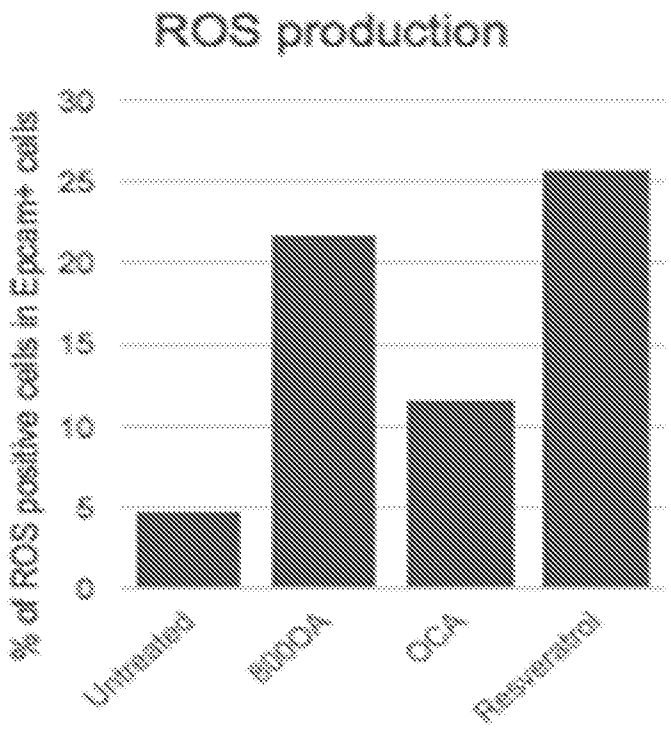
ROS production
% of ROS positive cells in Epcam+ cells
0
5
10
15
20
25
30
Untreated
EtOCA
OCA
Resveratrol

FIG. 10

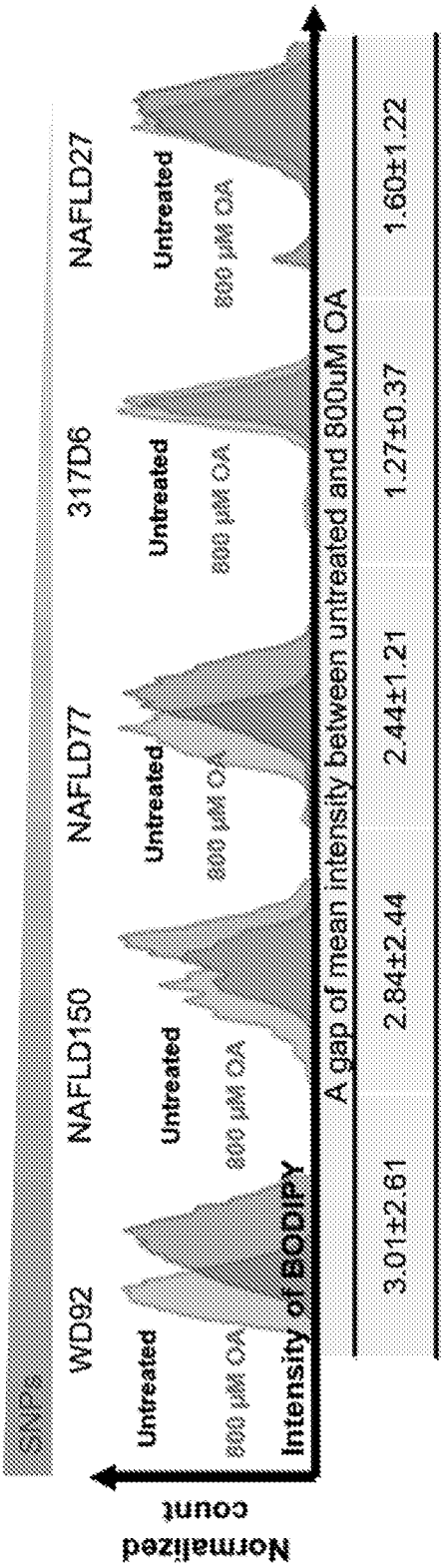
WD92
NAFLD150
NAFLD77
317D6
NAFLD27
Untreated
800 μM OA
Intensity of BODIPY
Normalized count
A gap of mean intensity between untreated and 800uM OA
3.01±2.61
2.84±2.44
2.44±1.21
1.27±0.37
1.60±1.22

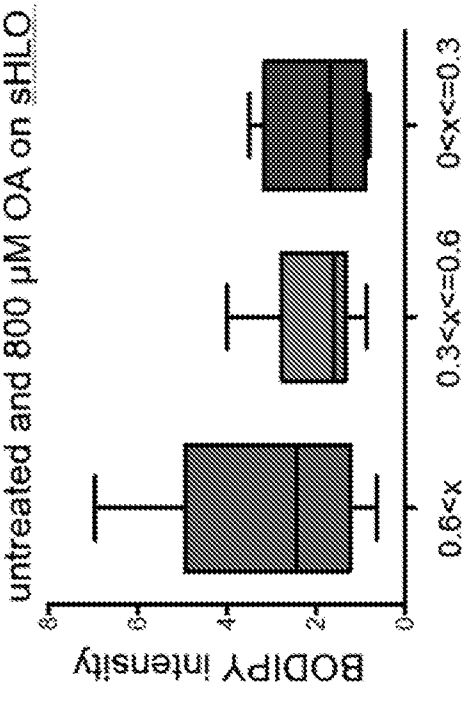
A gap of mean intensity between untreated and 800 μM OA on sHLO
BODIPY intensity
0
2
4
6
8
0.6<x
0.3<x<=0.6
0<x<=0.3

FIG. 11

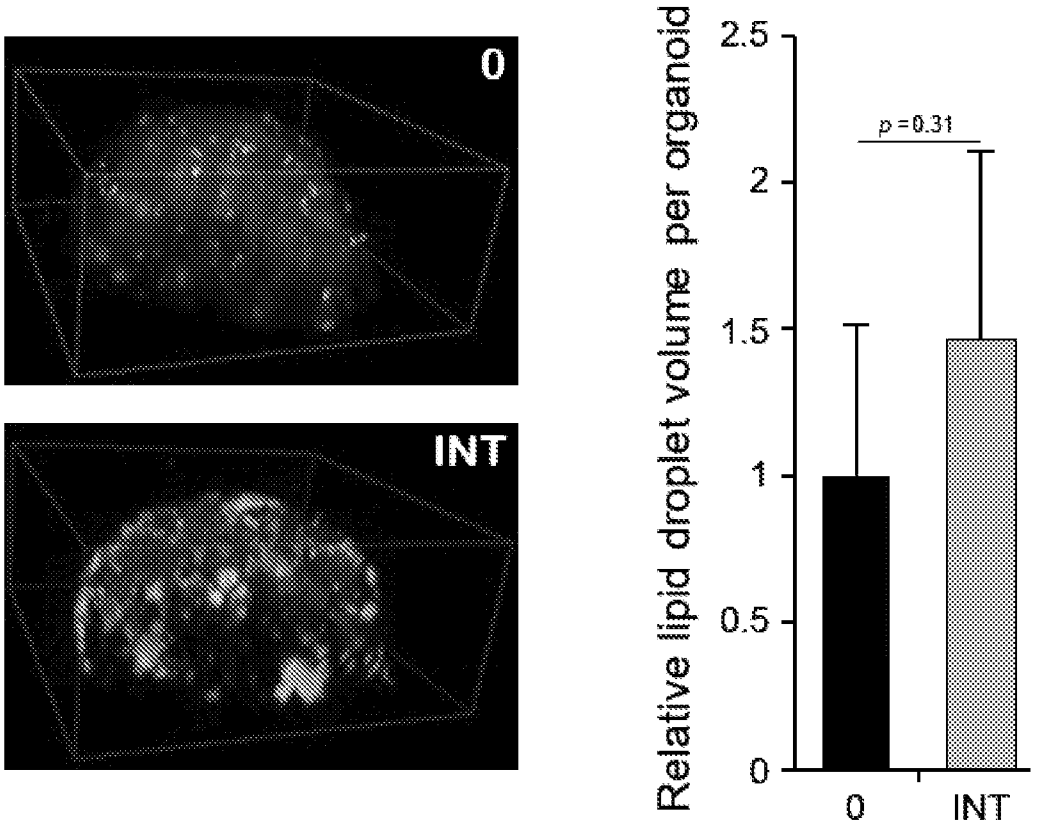
0
INT
Relative lipid droplet volume per organoid
2.5
2
1.5
1
0.5
0
p = 0.31
0
INT

FIG. 12

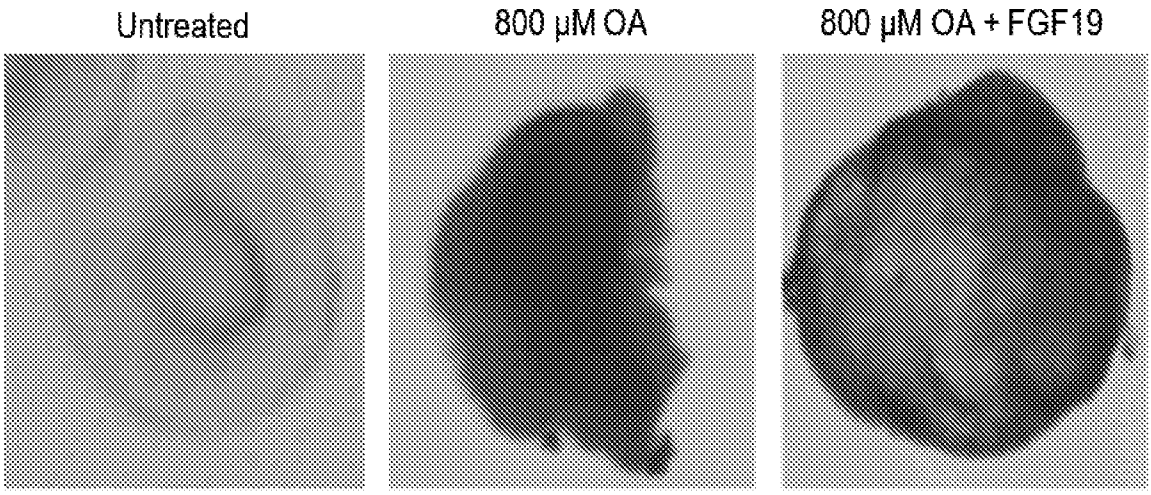
Untreated
800 µM OA
800 µM OA + FGF19

FIG. 13

INTERNATIONAL SEARCH REPORT

International application No.
PCT/US 17/59860

A. CLASSIFICATION OF SUBJECT MATTER
IPC(8) - A61L 27/00, C12N 5/00, C12N 5/071 (2017.01)
CPC - A61L 2300/252, A61L 27/54, A61L 27/52, A61L 27/3834, A61L 27/50

According to International Patent Classification (IPC) or to both national classification and IPC

B. FIELDS SEARCHED

Minimum documentation searched (classification system followed by classification symbols)
See Search History Document

Documentation searched other than minimum documentation to the extent that such documents are included in the fields searched
See Search History Document

Electronic data base consulted during the international search (name of data base and, where practicable, search terms used)
See Search History Document

C. DOCUMENTS CONSIDERED TO BE RELEVANT

Category*	Citation of document, with indication, where appropriate, of the relevant passages	Relevant to claim No.
X	Gori et al., "Investigating Nonalcoholic Fatty Liver Disease in a Liver-on-a-Chip Microfluidic Device", PLoS ONE 11(7): e0159729. doi:10.1371/journal.pone.0159729, 20 July 2016 (20.07.2016); entire document, especially pg 1 para 1-3, pg 2 para 2-5, pg 3 last para, pg 4 para 5, pg 5 para 3, pg 7 last para, pg 9 para 2-3, pg 12 para 3	1-10, 12
X	WO 2015/185714 A1 (Vrije Universiteit Brussel) 10 December 2015 (10.12.2015); entire document, especially pg 8 lines 17-21, pg 26 lines 14-20	11
A	Park et al., "Lipotoxicity of Palmitic Acid on Neural Progenitor Cells and Hippocampal Neurogenesis", Toxicological Research, 27(2), 103:110, June 2011 (06.2011); entire document	1-12
A	Nandivada et al., "Treatment of Parenteral Nutrition-Associated Liver Disease: The Role of Lipid Emulsions", Nutr vol. 4: 711-717, 2013, November 2013 (11.2013); entire document	1-12
A	Cabezas et al. "Nonalcoholic Fatty Liver Disease: A Pathological View", Nobumi Tagaya , ISBN 978-953-51-0853-5, 21 November 2012 (21.11.2012); entire document	1-12

☐ Further documents are listed in the continuation of Box C. ☐ See patent family annex.

* Special categories of cited documents:
"A" document defining the general state of the art which is not considered to be of particular relevance
"E" earlier application or patent but published on or after the international filing date
"L" document which may throw doubts on priority claim(s) or which is cited to establish the publication date of another citation or other special reason (as specified)
"O" document referring to an oral disclosure, use, exhibition or other means
"P" document published prior to the international filing date but later than the priority date claimed
"T" later document published after the international filing date or priority date and not in conflict with the application but cited to understand the principle or theory underlying the invention
"X" document of particular relevance; the claimed invention cannot be considered novel or cannot be considered to involve an inventive step when the document is taken alone
"Y" document of particular relevance; the claimed invention cannot be considered to involve an inventive step when the document is combined with one or more other such documents, such combination being obvious to a person skilled in the art
"&" document member of the same patent family

Date of the actual completion of the international search	Date of mailing of the international search report
22 December 2017	29 JAN 2018
Name and mailing address of the ISA/US Mail Stop PCT, Attn: ISA/US, Commissioner for Patents P.O. Box 1450, Alexandria, Virginia 22313-1450 Facsimile No. 571-273-8300	Authorized officer: Lee W. Young PCT Helpdesk: 571-272-4300 PCT OSP: 571-272-7774

INTERNATIONAL SEARCH REPORT

International application No.
PCT/US 17/59860

Box No. II Observations where certain claims were found unsearchable (Continuation of item 2 of first sheet)

This international search report has not been established in respect of certain claims under Article 17(2)(a) for the following reasons:

1. ☐ Claims Nos.:
because they relate to subject matter not required to be searched by this Authority, namely:

2. ☐ Claims Nos.:
because they relate to parts of the international application that do not comply with the prescribed requirements to such an extent that no meaningful international search can be carried out, specifically:

3. ☒ Claims Nos.: 13
because they are dependent claims and are not drafted in accordance with the second and third sentences of Rule 6.4(a).

Box No. III Observations where unity of invention is lacking (Continuation of item 3 of first sheet)

This International Searching Authority found multiple inventions in this international application, as follows:

1. ☐ As all required additional search fees were timely paid by the applicant, this international search report covers all searchable claims.

2. ☐ As all searchable claims could be searched without effort justifying additional fees, this Authority did not invite payment of additional fees.

3. ☐ As only some of the required additional search fees were timely paid by the applicant, this international search report covers only those claims for which fees were paid, specifically claims Nos.:

4. ☐ No required additional search fees were timely paid by the applicant. Consequently, this international search report is restricted to the invention first mentioned in the claims; it is covered by claims Nos.:

Remark on Protest

☐ The additional search fees were accompanied by the applicant's protest and, where applicable, the payment of a protest fee.

☐ The additional search fees were accompanied by the applicant's protest but the applicable protest fee was not paid within the time limit specified in the invitation.

☐ No protest accompanied the payment of additional search fees.